



Sedimentary facies analysis, seismic interpretation, and reservoir rock typing of the syn-rift Middle Jurassic reservoirs in Meleiha concession, north Western Desert, Egypt

Ahmed Rezk Hassan¹ · Ahmed A. Radwan¹ · Kamel H. Mahfouz¹ · Mahmoud Leila²

Received: 3 March 2023 / Accepted: 9 July 2023 / Published online: 21 July 2023
© The Author(s) 2023

Abstract

The Middle Jurassic syn-rift sediments of the Khatatba Formation contain not only the principle source rock organofacies in the north Western Desert (NWD), but also several potential sandstone reservoir targets. However, controls on the reservoir quality of the Khatatba facies and spatiotemporal evolution of the reservoir rock types (RRTs) are still blurred. This study integrates seismic, wireline logs, and conventional core data from some wells in the Meleiha development lease in the NWD to investigate the petrophysical characteristics of the Khatatba reservoir facies, and determine the different RRTs. On seismic, Khatatba Formation consists of high reflectivity, continuous reflections displaying an upward decrease in seismic amplitude corresponding to a fining-upward clastic succession of fluvial–tidal facies. These facies display a large-scale pore system heterogeneity, thereby comprising three different RRTs. RRTI and RRTII rocks have a well-connected pore network dominated by capillary and super-capillary pores ($> 10 \mu\text{m}$), whereas sub-capillary pores ($< 10 \mu\text{m}$) are more common in RRTIII sediments. RRTI rocks consist of quartzose sandstones with a clean pore network (cement $< 20\%$). The open pore system of RRTI allows a displacement of more than 80% of the pore water at entry pressure levels < 500 psi. Carbonate and clay components are more common in RRTIII rocks (average = 5.6% and 13%, respectively). These components adversely impact the pore system connectivity of RRTIII sediments. Fluvial channel sandstones host the principal fluid flow conduits where RRTI sandstones account for more than 95% of the reservoir flow capacity. The present study provides the first reservoir rock typing for the Khatatba clastic reservoir facies and highlights the link between depositional, compositional attributes and the spatial distribution of the different RRTs.

Keywords Middle Jurassic · Syn-rift sediments · Khatatba · Shushan Basin · Reservoir rock typing · Seismic interpretation · Petrophysics

List of symbols

K	Permeability (mD)
m	Cementation factor
PR_{\varnothing}	Pore size reduction (%)
PR_K	Permeability reduction (mD)
R_w	Formation water resistivity (OHMM)
R_{35}	Pore throat radius (μm)
S_w	Water saturation (%)
V_{sh}	Volume of shale (%)

\varnothing	Porosity (%)
\varnothing_{eff}	Effective porosity (%)

Abbreviations

AI	Acoustic impedance [$\text{g/ft (cm}^3 \text{ s)}$]
AEB	Alam El Bueib
DT	Sonic log ($\mu\text{s/ft}$)
FA	Facies association
FZI	Flow zone indicator
GR	Gamma ray log (API)
HFU	Hydraulic flow units
KH_IID	Khatatba Formation, IID member
LF	Lithofacies
LLD	Deep resistivity log (OHMM)
LLS	Shallow resistivity log (OHMM)
MF	Microfacies
MICP	Mercury injection capillary pressure (psi)
NPHI	Neutron log (%)

✉ Mahmoud Leila
mahmoud_lotfy@mans.edu.eg

¹ Department of Geology, Faculty of Science, Al-Azhar University, Assiut Branch, Assiut 71524, Egypt

² Department of Geology, Faculty of Science, Mansoura University, Mansoura, Egypt

NPI	Normalized porosity index
NWD	North Western Desert
PEF	Photo-electric factor log (b/e)
PTSD	Pore throat size distribution (μm)
QFL	Quartz–feldspars–lithic fragments
RC	Reflection coefficient
RHOB	Density log (g/cc)
RQI	Reservoir quality index (μm)
RRT	Reservoir rock typing
SCA	Special core analysis
SEM	Scanning electron microscopy
SMLP	Stratigraphic modified Lorenz plot
SSDS	Soft sediment deformation structures

Introduction

Reservoir rock typing (RRT) represents an essential approach for an optimized reservoir management. RRT approach encompasses a subdivision of reservoir facies into geologically distinctive units with predictable storage and flow capacities (Gunter et al. 1997; Guo et al. 2007; Masalmeh et al. 2012; El Adl et al. 2021; Leila 2019; Leila et al. 2022a, b; Radwan et al. 2021, 2022a, b). Therefore, a proper RRT should involve a full consideration for the initial depositional and diagenetic attributes, as well as their influence on the dynamic reservoir properties (Jooybari et al. 2010; Skalinski and Kenter 2014). Thus, depending solely on the conventional petrophysical measurements for RRT is unreliable. The initial step for accurate RRT should comprise a subdivision of the reservoir faces into distinctive units with specific geologically controlled petrophysical properties (static rock typing). This step is followed by a detailed analysis for the pore system characteristics and their impact on the fluid flow behavior within the reservoir facies (dynamic rock typing) (Skalinski and Kenter 2014; El Adl et al. 2021; Leila et al. 2023a, b; Elmahdy et al. 2023).

Initial depositional attributes often control the textural properties of the reservoir rocks (grain size and sorting) and thereby impact their original pore structure and geometry (e.g. Pittman 1992; Coskun et al. 1993). Additionally, the diagenetic processes (e.g. compaction, dissolution and cementation) commonly influence the pore connectivity, pore throat geometry, and therefore control both static and dynamic properties of the reservoir rocks (Houseknecht 1987; Pittman and Larese 1991; Coskun et al. 1993; Kim et al. 2007; Leila and Moscardiello 2019). Accordingly, a detailed analysis of the reservoir sedimentary facies, their fabric, composition as well as deciphering the link between depositional and diagenetic attributes is essential to understand the pore system evolution, and hence predict the static and dynamic properties of the reservoir rock types (RRTs).

Western Desert province hosting approximately 26.6% of the entire proven Egyptian hydrocarbon reserves is considered one of the most petroliferous hydrocarbon regions in North Africa (AlSharhan and Abd El-Gawad 2008; Yasser et al. 2021; Hassan et al. 2022). Western Desert accounts for a 54.8%, 44.1% and 17.5% of the Egyptian oil, condensate, and gas daily production, respectively (Hassan et al. 2022). These reserves mostly occur in the rift basins of the north Western Desert (NWD) (e.g. Shushan, Abu El-Ghradig; Fig. 1). These basins host several active petroleum systems in their syn- and post-rift sedimentary successions (AlSharhan and Abd El-Gawad 2008; El Diasty 2015; Abdelwahhab et al. 2022; Leila et al. 2022a, c; El Matboly et al. 2022; Saleh et al. 2023).

The present study focuses on boreholes from the Meleiha development lease, which lies in the southeastern part of Shushan Basin (Fig. 1). Recent oil, condensate, and discoveries in Shushan Basin (e.g. Jasmin, Emry fields) confirm the hydrocarbon prospectivity of the basin. Syn-rift organic-rich sediments of the Middle Jurassic Khatatba Formation represent the principle source for most oil and gas discoveries in Shushan Basin (Shalaby et al. 2011; Hassan et al. 2022; Leila et al. 2022a). The Khatatba organofacies charges multiple reservoir intervals within both syn- and post-rift successions (Dolson et al. 2001; AlSharhan and Abd El-Gawad 2008). Most studies about the NWD reservoirs were mainly focused on the post-rift Bahariya and late syn-rift Alam El Bueib formations (Kassab et al. 2019; Yasser et al. 2021; El Matboly et al. 2022). Leila et al. (2022a) reported a wide variability in sedimentary facies within the Khatatba Formation where the potential sandstone reservoir intervals are associated with the progradational and aggradational sedimentary successions. However, a detailed rock typing for the Khatatba clastics facies based on a comprehensive understanding for the spatiotemporal evolution of their pore system characteristics is still lacking. Therefore, this study applies an integrated petrophysical and sedimentological approach as a proxy to investigate the geologically controlled static and dynamic characteristics of the syn-rift clastics of the Khatatba Formation in the study region.

Geologic setting

NWD comprises a number of coastal basins stretching along the Mediterranean passive margin (Fig. 1). These basins were developed during the Early Mesozoic rifting of Gondwana landmass and opening of the Neotethys Ocean (Garfunkel 2004; Bosworth and Tari 2020; Torfstein and Steinberg 2020). The pre-rift sedimentary succession constitutes a Paleozoic clastic facies resting unconformably above the pre-Cambrian basement (Fig. 2; Schlumberger 1995; Zein El-Din et al. 2001). Rifting initially took place

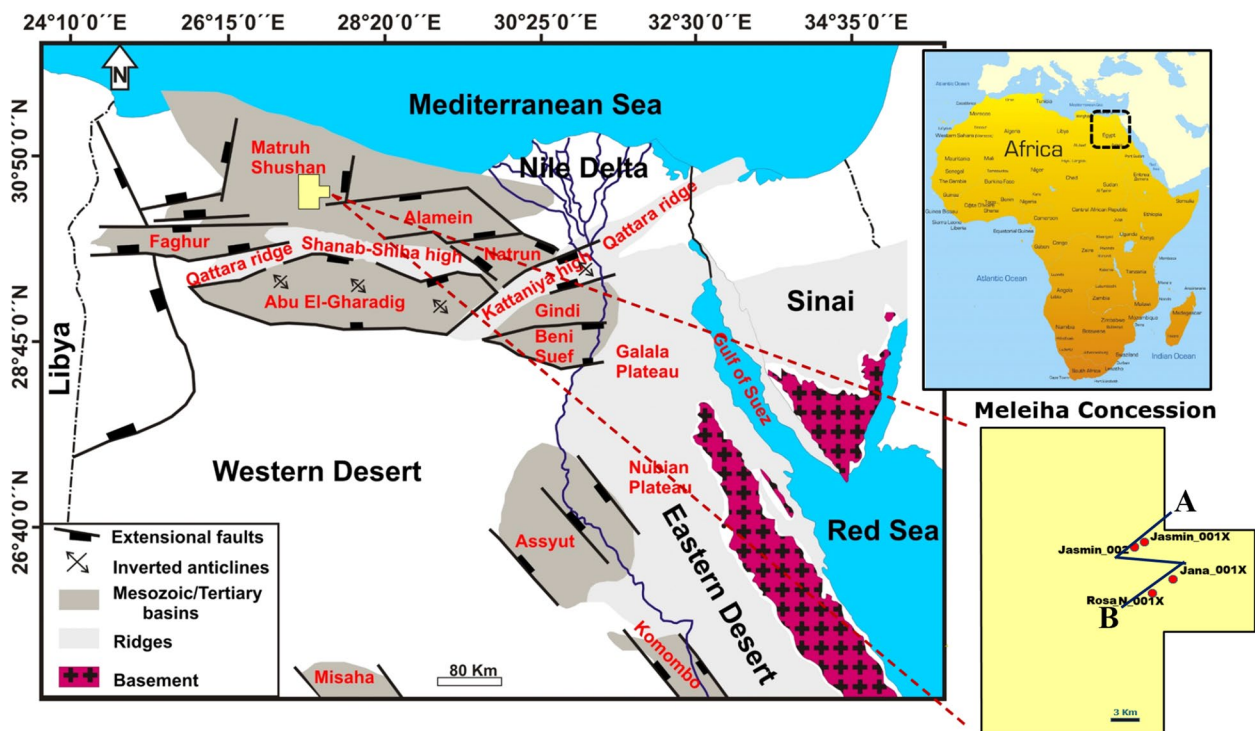


Fig. 1 Location map of the study area in southern part of Shushan Basin, north Western Desert, Egypt (modified after Bayoumi 1996)

during the Triassic and reached the peak by the Middle Jurassic (Dolson et al. 2001; Guiraud et al. 2005; Bosworth and Tari 2020). NWD basins were developed in a series of E–W, ENE–WSW, and NE–SW trending intracratonic half grabens with a dominant extensional fault patterns oriented NE–SW (Fig. 3). During Early Cretaceous, a major shift in the direction of the extension toward NE–SW took place, resulting in the development of complex fault patterns oriented NE–SW, NW–SE, and E–W (Dolson et al. 2001; Bosworth et al. 2008; Leila et al. 2022a).

The basin-fill stratigraphy of the NWD basins is similar and comprises three main tectono-stratigraphic units bounded by unconformity surfaces (Schlumberger 1995; Zein El-Din et al. 2001). The first unit comprises the Paleozoic clastic sequence of the continental and shallow marine Nubian sandstones and shales. The earliest Jurassic sediments consist of non-marine clastics of the Ras Qattara Formation that rest unconformably above the pre-rift Paleozoic facies (Fig. 2). Rift-related subsidence during Middle Jurassic triggered the accumulation of successive transgressive and regressive facies of the Khatatba Formation.

Khatatba Formation consists of deltaic and shallow marine sandstones, shales with interbedded coal seams (Keeley and Wallis 1991; Ayyad and Darwish 1996). Development of local depocenters near the major faults triggered the deposition of the Khatatba organic-rich facies, which act as the main source rock in the entire north Western Desert

(Dolson et al. 2001; El Diasty 2015; Abdelwahhab et al. 2022; El Matbouly et al. 2022; Leila et al. 2022a). Episodic variation in fault offsets during the deposition of the Khatatba Formation caused a wide lateral and vertical facies variability, and accumulation of a complex pile of successive prograding and retrograding facies (Leila et al. 2022a). Successive episodes of thermal subsidence and stretching prevailed during the Late Jurassic allowed the deposition of shallow-water carbonates (Masajid Formation) conformably above the Khatatba clastics. Masajid carbonates are capped by the Cimmerian unconformity. The latter documents a widespread inversion phase coupled with tilting, partial erosion, and karstification of the Jurassic succession (Keeley et al. 1990; Keeley and Wallis 1991). This unconformity is paved by shallow marine mixed siliciclastic–carbonate facies of the Lower Cretaceous Alam El Bueib (AEB) Formation.

The post-rift unit includes the Upper Cretaceous continental and coastal marine clastics (Bahariya Formation), and the transgressive marine shales, carbonates (Abu Roash Formation). This transgressive sedimentation was terminated by the Late Cretaceous compression induced by the convergent movement between African and Eurasian plates, which lasted until the Late Eocene (Guiraud and Bosworth 1997; Bosworth et al. 2008). This was accompanied by a phase of tectonic inversion which developed several inverted structural patterns extending as fold belts across the whole NWD. Therefore, the Late Cretaceous

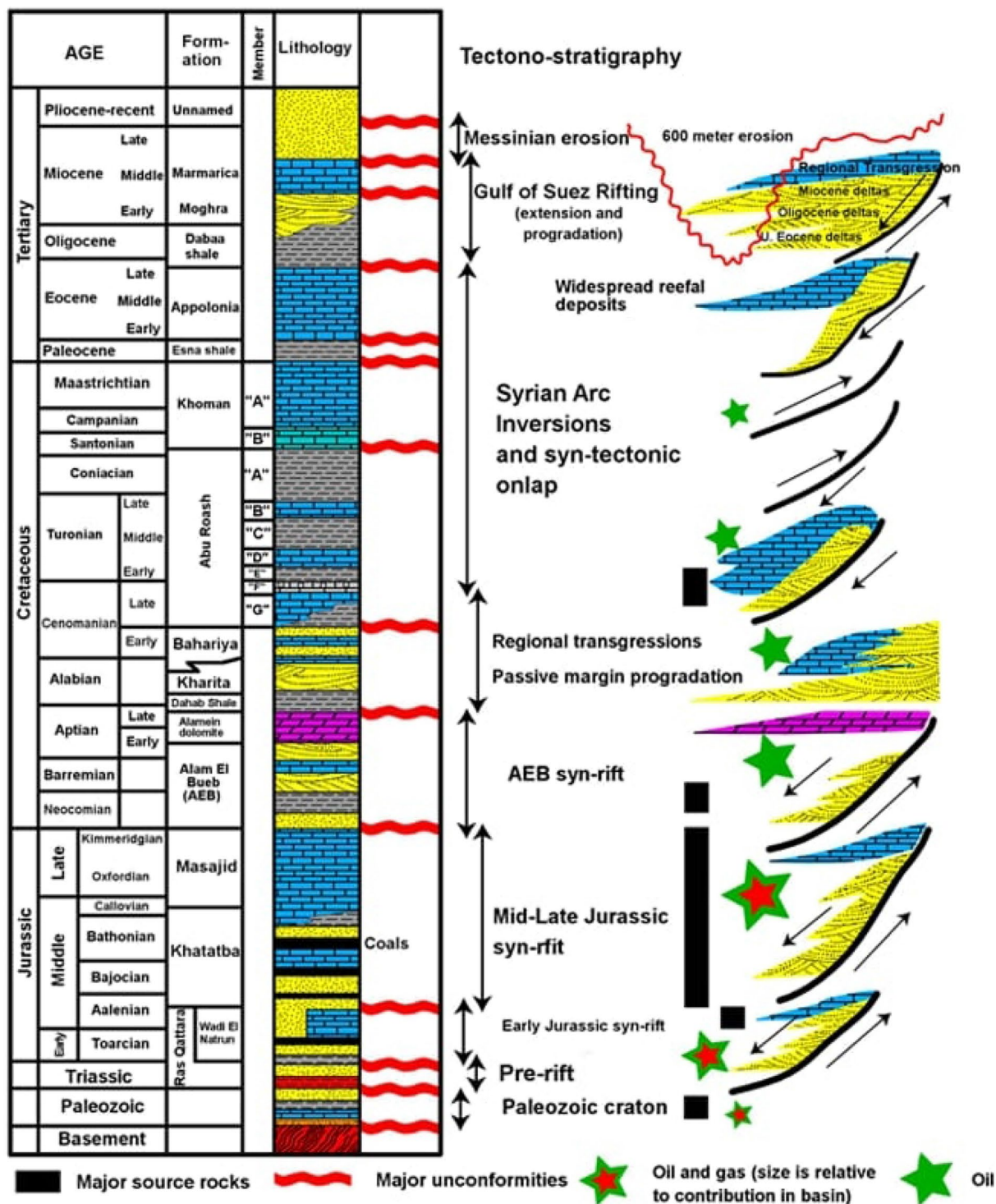


Fig. 2 Generalized lithostratigraphic column of the study region illustrating the tectono-stratigraphic evolution of the Shushan basin-fill sedimentary succession (Schlumberger 1995; Wescott et al. 2011)

Abu Roash Formation is unconformably followed by thin sedimentary successions of mixed marine and non-marine Paleogene–Neogene facies (EGPC 1994; Dolson et al. 2001; Zein El-din et al. 2001).

Data and methods

The present study is based on a diverse subsurface dataset including 2D seismic, borehole logs, and conventional cores

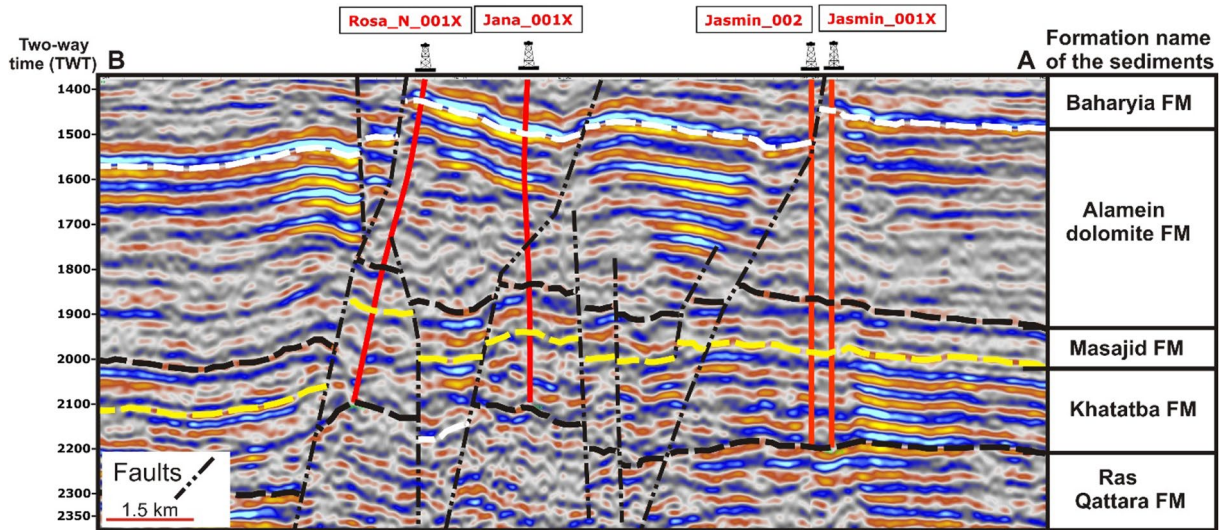


Fig. 3 Interpreted 2D seismic profile passing through the studied wells illustrating the main structural patterns affecting the study region (profile location A-B is illustrated in Fig. 1)

from the Eastern part of Meleiha Concession, Shushan Basin in the NWD (Fig. 1). The seismic data comprises a grid of twenty 2D seismic profiles covering an area of approximately 67.16 km². Seismic profiles were interpreted in order to define the main structural patterns in the study region. The

procedure of seismic data interpretation starts with tying seismic to well data (Fig. 4). The stratigraphic horizons were then picked and mapped. The interpretation of top Khatatba was picked below the Masajid carbonate horizon which is characterized by its high reflectivity and strong positive

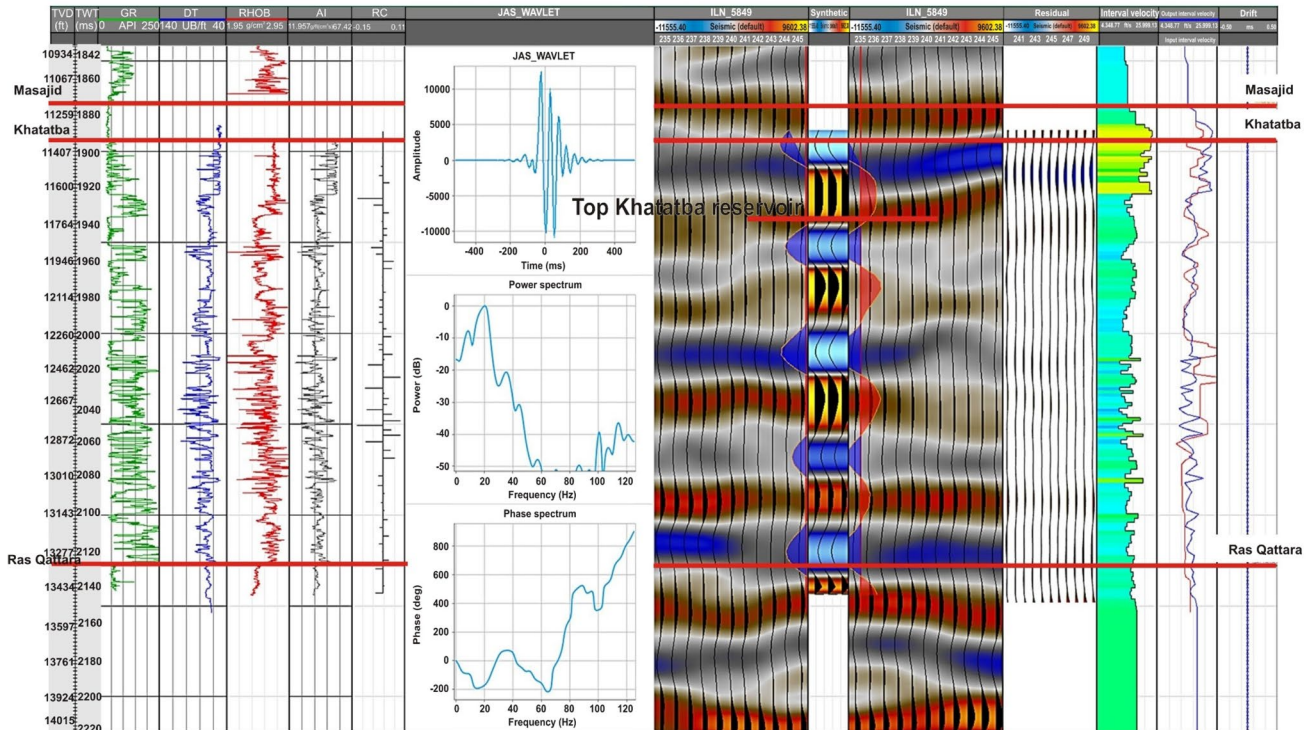


Fig. 4 Synthetic seismogram illustrating tying of seismic to well data by computing the reflectivity coefficient from density and sonic logs. The seismogram shows a good correlation between the studied stratigraphic horizons and well data

amplitude (peak) (Fig. 4). A complete suite of wireline logs for the studied wells were utilized to define the hydrocarbon bearing pay zones within the studied Khatatba succession.

Sedimentary facies analysis

Analysis of sedimentary facies is based on a detailed sedimentological description of the available 63-ft-thick conventional core interval retrieved from the Middle Jurassic Khatatba sedimentary succession in Jasmin_002 well (12,262–12,325 ft). The analysis involved a sedimentological core description based on identification of the lithological characteristics and sedimentary structures. The different lithofacies were then grouped in sedimentary facies associations accumulated within specific depositional environments.

Petrography and microfacies analysis

A total of 26 thin sections were prepared from the conventional and side wall core plugs retrieved from the Khatatba clastic interval in Jasmin_002 and Jasmin_001X wells, respectively. The thin sections were prepared in Corex laboratories, Egypt. Prior to microscopic examination, the thin sections were stained with blue dye, potassium ferricyanide, Alizarin Red-S, and sodium cobalt nitrate for the identification of porosity, carbonate, and feldspars mineral phases, respectively (Houghton 1980). The thin sections were then studied under the plane polarized microscope to determine their modal composition as well as the relative abundance of each component using the standard point counting scheme of Dickinson (1970). Scanning electron microscopy (SEM) was performed on the gold-coated polished thin sections to identify the pore structure as well as the morphology and distribution of different pore-occluding cements. Microfacies analysis was performed based on the modal composition of each thin section as well as the relative abundance of different detrital and authigenic mineral phases (e.g. Blatt and Tracy 1996).

Wireline logging interpretation

The available wireline logs including radioactivity logs (gamma ray GR), acoustic logs (sonic DT), electrical resistivity logs (LLS, LLD) as well as neutron (NPHI), density (RHOB), and photo-electric factor (PEF) logs from Jasmin_002 well were utilized in this study. The wireline logs were analyzed and processed using Techlog software (TL.2015.3). Shale content in the Khatatba sandstones was computed using a single-log method (gamma ray), whereas the density-neutron combination was applied to calculate porosity values (Yasser et al. 2021; Abdelmaksoud and Radwan 2022; Radwan et al. 2022a, b; Radwan and Nabawy

2022). Based on the obtained shale volume values, water saturation (S_w) was deduced using Indonesian equation which is more appropriate for S_w calculations in shale-rich reservoirs (Poupon and Leveau 1971). Formation water resistivity (R_w) and cementation factor (m) values in the studied Khatatba sediments were deduced using Pickett plot (Pickett 1972). Hydrocarbon-bearing intervals were interpreted using theoretical cutoff values of 35% for shale volume (V_{sh}), 7% for effective porosity (\varnothing_{eff}), and 65% for water saturation (S_w).

Routine and special core analysis

Routine core analysis (RCA) involves the measurement of porosity, permeability, and grain density of 56 cylindrical core plugs retrieved from the Khatatba pay zone interval in Jasmin-002 well. RCA measurements were performed in Corex laboratories, Egypt, using helium gas expansion porosimeter and nitrogen permeameter for measuring the porosity (\varnothing) and permeability (K), respectively. Prior to RCA measurements, the core plugs were cleaned with distilled water and dichloromethane to remove the drilling fluids and hydrocarbon residues. Porosity and permeability measurements were performed on clean dry plugs under an ambient pressure of 400 psi. According to Amaefule et al. (1993), the measured \varnothing – K values were utilized to investigate the reservoir performance, quality, and heterogeneity. Amaefule scheme involves the calculation of flow zone indicator (FZI in μm), reservoir quality index (RQI in μm), and normalized porosity index (NPI in decimals) as functions of porosity (\varnothing , in decimals) and permeability (K , in millidarcy mD) as follows:

$$\text{FZI} = \text{RQI}/\text{NPI} \quad (1)$$

$$\text{NPI} = \varnothing/(1 - \varnothing) \quad (2)$$

$$\text{RQI} = 0.0314 \times \sqrt{(K/\varnothing)} \quad (3)$$

Additionally, effective pore throat radius (R_{35}) values are calculated as function of the obtained \varnothing – K values for each plug sample. The R_{35} was calculated to delineate the effect of pore sizes on the reservoir quality as follows Winland (1972):

$$\text{Log}(R_{35}) = 0.732 + 0.588 \text{ log}(K) - 0.864 \text{ log}(\varnothing) \quad (4)$$

where R_{35} represents the pore throat radius at 35% mercury saturation.

Special core analysis (SCA) was carried out on 5 samples in order to investigate their pore system characteristics (e.g. pore throat size geometry, distribution, and connectivity) (Rose and Bruce 1949; Swanson 1981; Wells and Amaefule

1985; Vavra et al. 1992). SCA involves the measurement of mercury injection capillary pressure (MICP) following the analytical procedure of Leverett (1941) and Vavra et al. (1992). The impact of incremental increase in confining pressure (from 400 up to 8000 psi) on \varnothing - K values was also investigated as follows:

$$PR_{\varnothing} = \varnothing - \varnothing_{6000-8000}$$

$$PR_K = K - K_{6000-8000}$$

where PR_{\varnothing} and PR_K are the reduction in pore size and permeability due to confining pressure. \varnothing and K are the measured porosity and horizontal permeability values at ambient pressure (~ 400 psi), while $\varnothing_{6000-8000}$ and $K_{6000-8000}$ represent the measured values at confining pressure levels of 6000 and 8000 psi.

Results and interpretations

Seismic interpretation

The boundary between syn-rift Masajid carbonate and the underlying Khatatba clastics is represented by a paramount shift in seismic polarity with an abrupt decrease in acoustic impedance. Top Khatatba Formation is characterized by an

abrupt increase in seismic reflectivity (Figs. 3, 4). The Khatatba seismic facies consists of parallel, continuous seismic reflections with high reflectivity and amplitude. The latter vary vertically and laterally in the study region. Khatatba seismic reflections display a lateral decrease in seismic amplitude toward the southwest direction where their configuration changes from a prograding, and well-bedded to a slightly chaotic typifying a lateral variation in depositional facies. The studied wells were drilled in order to target the well-bedded reflections which display an upward decrease in seismic amplitude. The depth to top of the Khatatba Formation varies greatly with a general dipping in the southwestern part of the study region (Fig. 5). Structural highs adjacent to the major faults form several four-dip way closure structures in the central and southeastern parts of the study region. The thickness of the Khatatba Formation increases northward where a maximum value of > 1800 ft is observed in the northwestern part of the study area (Fig. 6).

Sedimentary lithofacies and facies associations

Seven sedimentary lithofacies were identified in the studied cored interval of the Khatatba Formation (Fig. 7). Massive mudstone (LF1) is represented by structureless thin beds of dark gray to black mudstone. LF1 is common at the base of the cored interval reaching a maximum thickness of ~ 0.5 ft (15 cm). In other parts, LF1 beds display a thickness of less

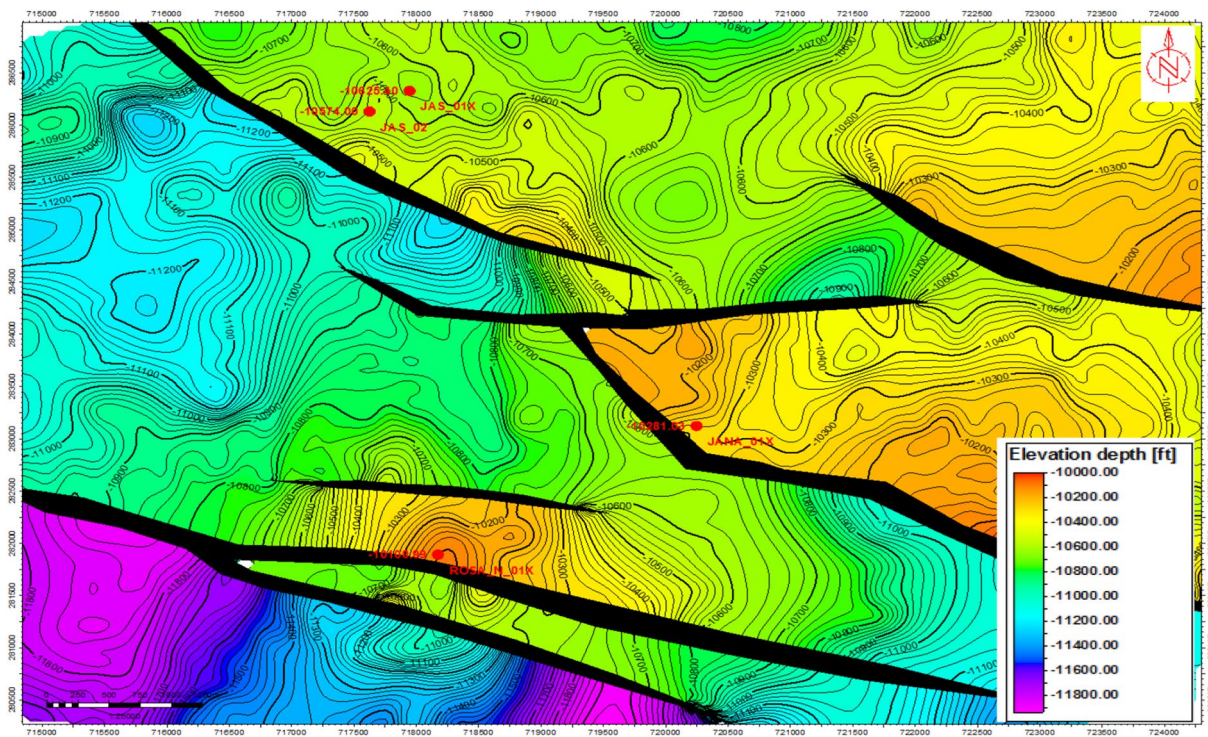


Fig. 5 Depth contour map to the top of the Khatatba Formation typifies a general dipping toward the southwestern part of the study region

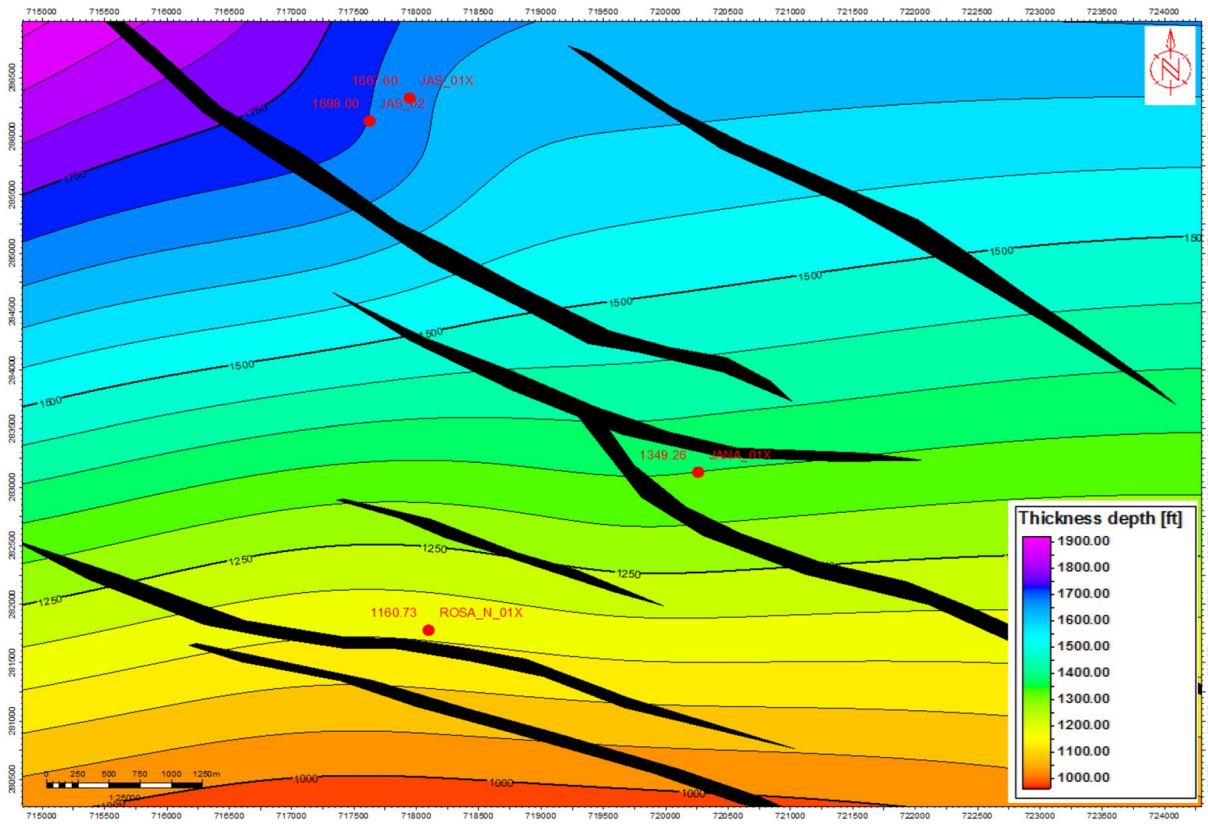


Fig. 6 Thickness contour map of the Khatatba Formation in the study area illustrating a general increase in thickness northward

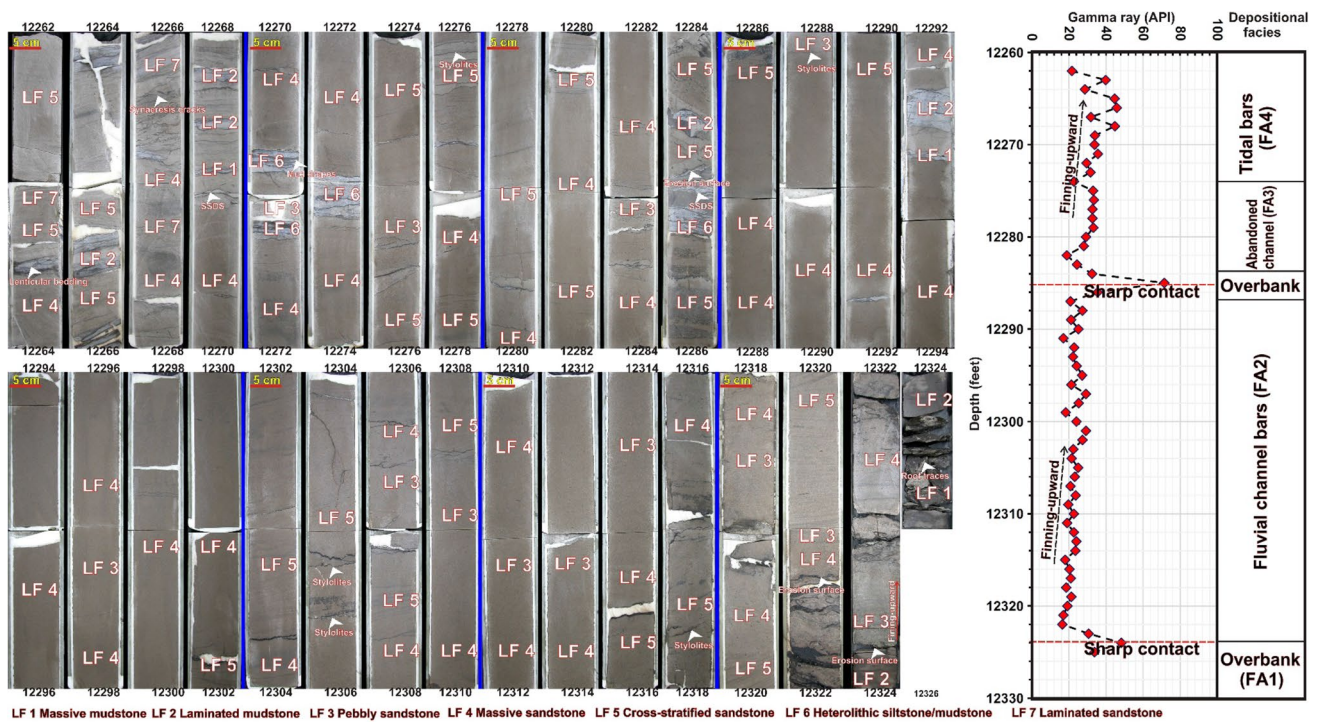


Fig. 7 Interpretation of sedimentary lithofacies, facies association, and sedimentary patterns encountered in the cored interval of the Khatatba Formation in Jasmin_002 well

than 5 cm. LF1 beds have a massive appearance and are slightly bioturbated with rootlets (Fig. 7). Laminated mudstone (LF2) comprises medium to dark gray sharp-based, planar-, cross-laminated, and non-bioturbated mudstone beds. LF2 beds range in thickness from ~3 to 7 cm, and they are more common in the upper part of the cored interval. Pebbly sandstone (LF3) encompasses approximately 20% of the studied cored interval. LF3 sandstone beds are mainly structureless except an occasional occurrence of planar cross-stratifications. Beds of LF3 range in thickness from a few centimeters up to 1 m, and they are more frequent in the lower part of the cored interval where they occur in stacked in fining-upward patterns. LF3 beds often contain dark irregular stylolites (Fig. 7).

Massive sandstone (LF4) consists of light gray structureless beds. LF4 sediments are often associated with LF3 in the lower part of the cored interval. LF4 beds also display gradational bases and tops and range in thickness from several centimeters up to 2 m, thereby comprising more than 25% of the studied cored interval. Sedimentary structures and bioturbation are absent, however, irregular dark stylolites are frequently present. Cross-stratified sandstone lithofacies (LF5) consists of light gray, coarse-grained sandstones stacked in fining-up patterns which comprise ~40% of the investigated cored interval. LF5 beds are stratified with thin (~1–3 cm) tabular cross-beds sets. LF5 sandstone beds range in thickness from few centimeters up to several decimeters and are often associated with LF3 and LF4 sandstones (Fig. 7).

Heterolithic siltstone/mudstone lithofacies (LF6) is made of medium gray siltstones interlaminated with mudstones and very fine-grained sandstones. LF6 sediments are only present in the upper part of the cored interval. LF6 beds

often display sharp bases and tops (Fig. 7). LF6 beds are thin (<5 cm), and contain lenticular and flaser bedding with thin flat siltstone lenses interlaminated with mud drapes and ripple laminations. Soft sediment deformation structures (SSDS) are frequently observed in LF6 beds (Fig. 7). Laminated sandstone lithofacies (LF7) is localized in the uppermost part of the studied cored interval. LF7 sandstones consist of medium gray, fine-grained argillaceous sandstones cross-laminated with thin (<1 cm) pinstripe laminae. LF7 beds range in thickness from 3 to 10 cm and are commonly associated with LF6 and LF5 sediments.

Based on the sedimentary characteristics of the different lithofacies and their vertical stacking patterns, several sedimentary facies associations were identified in the studied cored interval of Khatatba Formation. The studied intervals are dominated by fluvial facies at the base grading upward into tidally influenced sediments (Fig. 8). The base of the studied succession consists of fluvial facies made of overbank mudstones followed by fluvial channel-fill sandstones. The fluvial overbank facies (FA1) consists of alternated massive and laminated mudstone lithofacies (LF1, LF2). The mudstones are sparsely bioturbated by small root traces. These characteristics confirm the deposition of these mudstones in a continental, subaerial conditions likely in a floodplain environment as a channel overbank facies (e.g. Varejão et al. 2021; Leila et al. 2022a, b).

Fluvial channel sandstone bars (FA2) comprise amalgamated beds of pebbly (LF3), massive (LF4) and cross-stratified sandstones (LF5). FA2 is erosionally-based, and the erosion surface is mantled by pebbly sandstone beds (Fig. 7). FA2 sandstones are stacked in a successive fining-upward patterns where the pebbly sandstone lithofacies is often followed by interbedded massive and cross-stratified

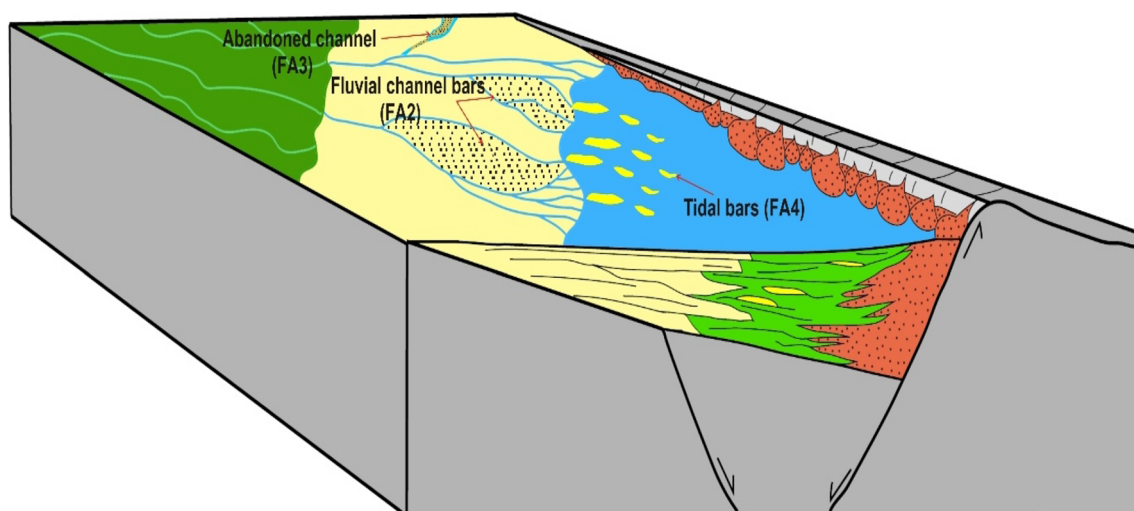


Fig. 8 A depositional model (not to scale) illustrating the depositional setting of the studied sedimentary facies encountered in the cored interval of the Khatatba Formation in the study region

sandstones. Multiple erosion surfaces are locally observed reflecting a repeated channel cut and fill episodes. The fluvial channel-fill sandstones are amalgamated and stacked-vertically forming a thick succession ~40 ft of fluvial channel sand bars (Bridge 2006; El Adl et al. 2021; Leila et al. 2022a, b). The gamma ray values of FA2 sandstones are generally low (20–30 API) and display successive bell-shaped patterns. The sandstones are non-bioturbated with very low mud content. FA2 has a massive appearance where the sedimentary structures are only represented by tabular low-angle cross-beds sets in the cross-stratified sandstone lithofacies (LF5). Basal erosion surface, repeated cut and fill structures, and the fining-upward sandstone patterns confirm in-channel deposition of FA2 sandstones in a fluvial environment (Fig. 8). Moreover, the coarse-grained sandstones with very low mud content and absence of bioturbation suggest the deposition of FA2 sandstones by high energy fluvial channels (Miall 1977; Tucker 2001).

Abandoned channel facies (FA3) occurs at the upper part of the studied succession. FA3 comprises an erosion-based association of massive and laminated sandstone lithofacies (LF4, LF7) interbedded with heterolithic siltstone/mudstone (LF6), and cross-stratified sandstones (LF5). FA3 sediments display a fining-upward trend where the coarse-grained cross-stratified and massive sandstones grade upward into fine-grained laminated sandstones and heterolithic siltstone/mudstone sediments (Fig. 7). FA3 sediments are non-bioturbated. The fining-upward erosion-based association, upward increase in mud content, general absence of bioturbation, and occurrence of cross-stratified fine-grained sandstones suggest deposition of FA3 in a low-energy abandoned fluvial channel environment (Baker 1987; Miall 1996; Walling and Hu 1998).

Tidal bars facies association (FA4) occurs at the uppermost part of the studied interval (Fig. 7). FA4 consists of interbedded medium and fine-grained laminated sandstones (LF7), heterolithic siltstone/mudstone, massive and laminated mudstone (LF1, LF2). Fine-grained massive and cross-stratified sandstones (LF4, LF5) are also present in the upper part of FA4. The lithofacies of FA4 display serrated gamma ray motifs reflecting a sharp variation in the sand/mud ratio. Syneresis cracks, low-angle cross, and lenticular beddings as well as mud drapes are frequently present. These sedimentary features suggest deposition of FA4 during periods of slack water conditions. Common occurrence of mud drapes and lenticular beddings demonstrates the tidal influence on FA4 sedimentation. Additionally, the presence of syneresis cracks points to a subaqueous deposition with periodic variation in salinity (Fig. 8; Nio and Yang 1991; Bhattacharya and Walker 1991; Leila and Moscardiello 2019; El Adl et al. 2021; Leila et al. 2022a, b).

The interpreted fining-upward fluvial–tidal succession corresponds to the well-bedded seismic facies in the study

region. The upward decrease in seismic amplitude and reflectivity coincides with the upward decrease in fluvial, and increase in tidal influence coupled with increase in the mud content.

Petrography and microfacies

The Khatatba sandstones are grain-supported with low content of matrix. Based on the modal composition and relative abundance of quartz, feldspars, and rock fragments, the Khatatba sandstones were classified as quartz arenite. The sandstones display an average composition of $Q_{97.8}F_{1.9}L_{0.25}$ (Fig. 9). They contain variable contents of authigenic mineral phases, and therefore, five sandstone microfacies have been observed.

Quartz arenite (MF1)

Quartz arenite is the most common microfacies in the studied Khatatba sandstones. The detrital framework grains of MF1 are dominated by rounded to sub-angular quartz grains (average = 74%) (Table 1). Matrix content is very low, and MF1 consists mainly of quartz, while other detrital and authigenic mineral phases are relatively rare (Fig. 10a). Feldspars (average = 1.49%) are mainly K-feldspars. MF1 is moderately to strongly compacted where the grain-to-grain contacts are mainly sutured and concavo-convex. Syntaxial quartz overgrowth (Fig. 11a) and silica cement are the most common authigenic mineral phases in MF1 (average = 5.8%). Carbonate (mainly dolomite) and clay materials (mainly kaolinite) are also common authigenic mineral phases in MF1 (average = 2.75% and 9.1%, respectively). Large intergranular pores are observed and have good connectivity, and therefore, MF1 sandstones have a well-connected pore network (Fig. 10a).

Dolomitic quartz arenite (MF2)

MF2 sandstones comprise a carbonate-rich quartz arenite. MF2 consists of detrital quartz and carbonate cement. Quartz grains are slightly compacted with long and point grain-to-grain contacts. Quartz grains are angular to sub-rounded and are partly coated with clays. Feldspars are represented by slightly dissolved K-feldspars (Fig. 10b, c). Carbonate cements (average = 8.22%) are represented by emerging patches of pore-filling ferroan dolomite (Fig. 10b, c). Quartz overgrowth and silica cement are also common (average = 2.89%). The intergranular pores are mainly filled with carbonate cement, and therefore, MF1 pore network is partly blocked where the size of most pore throats is smaller than that in MF1.

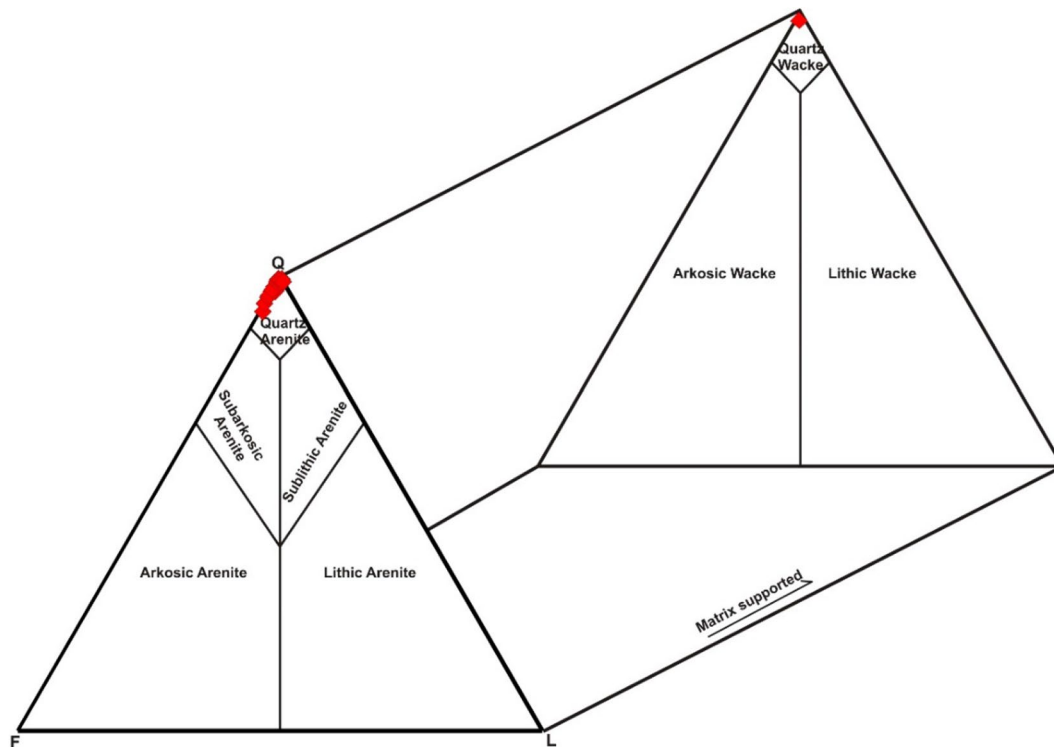


Fig. 9 Quartz–feldspars–lithic fragments (QFL) ternary plot shows the modal classification of the Khatatba sandstones (interpretation fields from Blatt and Tracy 1996)

Kaolinitic quartz arenite (MF3)

Kaolinitic quartz arenite (MF3) is made of rounded to sub-angular quartz grains and partly dissolved *K*-feldspars (Fig. 10d, e). MF3 is moderately compacted with abundant point and long grain-to-grain contacts. Detrital clay matrix is also abundant, and the intergranular pores are mainly filled with kaolinite (Fig. 11b). Other common authigenic phases comprise silica cement (average = 2.3%) and pyrite (average = 2.8%) (Table 1). Intergranular pores are represented by scattered isolated pores (dead ends) (Fig. 10e). Dissolution secondary pores are also reported due to the partial leaching of feldspars (Fig. 10d).

Quartz wacke (MF4)

MF4 sandstones consist of fine to medium-grained, well-sorted, sub-rounded quartz grains. Feldspars and rock fragments are rarely observed. The framework grains are coated with clays (Fig. 10f). Authigenic phases are mainly calcite (average = 3.17%), quartz overgrowth (average = 5), and pyrite (average = 3%) (Table 1). No intergranular pores were observed as the clay matrix materials completely infill the intergranular volume (Fig. 10f). Clays in MF4 occur as massive, loose aggregates and occasionally form thin coatings around the detrital framework grains. Clays also form thin

lamina distributed parallel to the detrital quartz grains (clay cutans). Such distribution of clays points to their dominant detrital origin where the syndepositional suspended clays were preferentially settled in the pore spaces during the deposition (e.g. De Ros et al. 1994; Leila and Moscariello 2019).

Wireline logging results

The cored interval of the Khatatba Formation in Jasmin_002 well displays a notable upward increase in gamma ray values consistent with the upward transition from fluvial to tidal environment. The fluvial channel sandstone bars at the base have shale volume values < 20%. On the other hand, the overbank and abandoned fluvial channel facies display the highest shale volume values ~ 60% (Fig. 12). Movable hydrocarbons preferentially occur in the fluvial channel sandstone bars displaying the highest values of effective porosity > 10% (Fig. 12). This is correlated with a high-amplitude seismic peak corresponding to the top reservoir interval (Fig. 4). Similarly, the calculated permeability decreases upward with highest values ~ 100 mD observed in the fluvial channel and tidal bars. Water saturation increases upward where the greatest water saturation and lowest hydrocarbon saturation values are, respectively, observed in the overbank and abandoned fluvial channel facies. The prominent separation

Table 1 Petrographic modal composition of the Khatatba sandstone microfacies

Components (%)	Quartz arenite microfacies (MF1) (n = 18)			Dolomitic quartz arenite microfacies (MF2) (n = 3)			Kaolinitic quartz arenite microfacies (MF3) (n = 3)			Quartz wacke microfacies (MF4) (n = 2)		
	Minimum	Maximum	Average	Minimum	Maximum	Average	Minimum	Maximum	Average	Minimum	Maximum	Average
<i>Detrital and authigenic components</i>												
Quartz	62	89.5	74	69	81	74	69	81	74	55	65	60.16
L. fragments	0	0.5	0.12	0	0.67	0.4	0	1	0.33	0	0	0
Feldspars	0	4.81	1.5	0.5	0.8	0.6	0	3.33	1.11	0.33	2	1.16
Glauconite	0	3.33	0.43	0	6.3	2.27	0.33	1.33	0.88	0	0	0
Quartz cement	0.5	15	5.8	1.5	4.67	2.9	0	6	2.33	4	6	5
Carbonate cement	0	11.3	2.75	6.5	11.5	8.22	0	1.33	0.44	1.67	4.67	3.17
Pyrite	0.5	7.3	2.65	0.5	5.67	2.39	0.5	6	2.83	2.67	3.33	3
Clays	2.3	14	9.1	2	6.66	4.39	13.3	14	13.6	14.33	36.33	25.33
Heavy minerals	0	1.5	0.33	0	0.5	0.33	0	1.3	0.43	0	2.33	1.16
Point count porosity	0	8	3.01	1.3	4.0	2.27	1.5	5.67	3.94	0	2	1

between shallow and deep resistivity logs in the fluvial channel and tidal bar facies reveals the presence of movable hydrocarbons within the Khatatba pay zone where the hydrocarbon saturation reaches up to 79%. Thus, the pay zone thickness and connectivity are largely dependent on the vertical distribution and architecture of sedimentary facies and reservoir rock types (RRTs).

The neutron-density cross-plot reveals the dominant sandstone matrix composition of the Khatatba sediments (Fig. 13). Notably, the samples of fluvial channel sandstone bars are plotted on and above the sandstone line confirming their clean quartzose composition with minimal contents of clays and carbonate phases. The upward deviation from the sandstone line is mostly attributed to the occurrence of movable hydrocarbons.

Pore system of the Khatatba sediments

The petrophysical properties and pore system characteristics vary greatly among the studied Khatatba sedimentary facies (Table 2). This aligns with the petrographic observation which demonstrated a heterogeneous pore system ranging from a well-connected intergranular network in the quartz arenite microfacies “MF1” to a tight pore system with no visual intergranular pores in quartz wacke microfacies “MF4.” The measured RCA data show elevated values of horizontal permeability in the fluvial channel bars (average = 250 mD). The fluvial channel bars sandstones have permeability values tenfold greater than those in other sedimentary facies. Helium porosity values are also greater in fluvial channel bars sandstones than in the other sedimentary facies. However, the average porosity values in the Khatatba sedimentary facies vary in a narrow range from 9.04 to 14.06%. Thus, the wide variation in permeability among the studied sedimentary facies is related to variation in pore structure and geometry rather than the pore volume.

The reservoir quality index (RQI) values confirm a good reservoir quality for the fluvial channel bars sandstones with average RQI ~ 1 μm , whereas the average RQI values in the other sedimentary facies are less than 0.5 μm . Similarly, flow zone indicator (FZI) typifies occurrence of excellent fluid flow zones only in the fluvial channel bars (average > 5 μm). Additionally, pore throat radius (R_{35}) values greater than 10 μm are restricted to the fluvial channel bars sandstones, while the other sedimentary facies display average R_{35} values < 4 μm (Table 2).

Porosity-horizontal permeability cross-plot demonstrates a wide variation in the pore system network among the studied sedimentary facies. Sandstones of the fluvial channel bars have high porosity and permeability, where the latter increases with increasing porosity values which are mostly above 15% typifying a pore system dominated by well-connected pore channel network (Fig. 14a). Other sedimentary

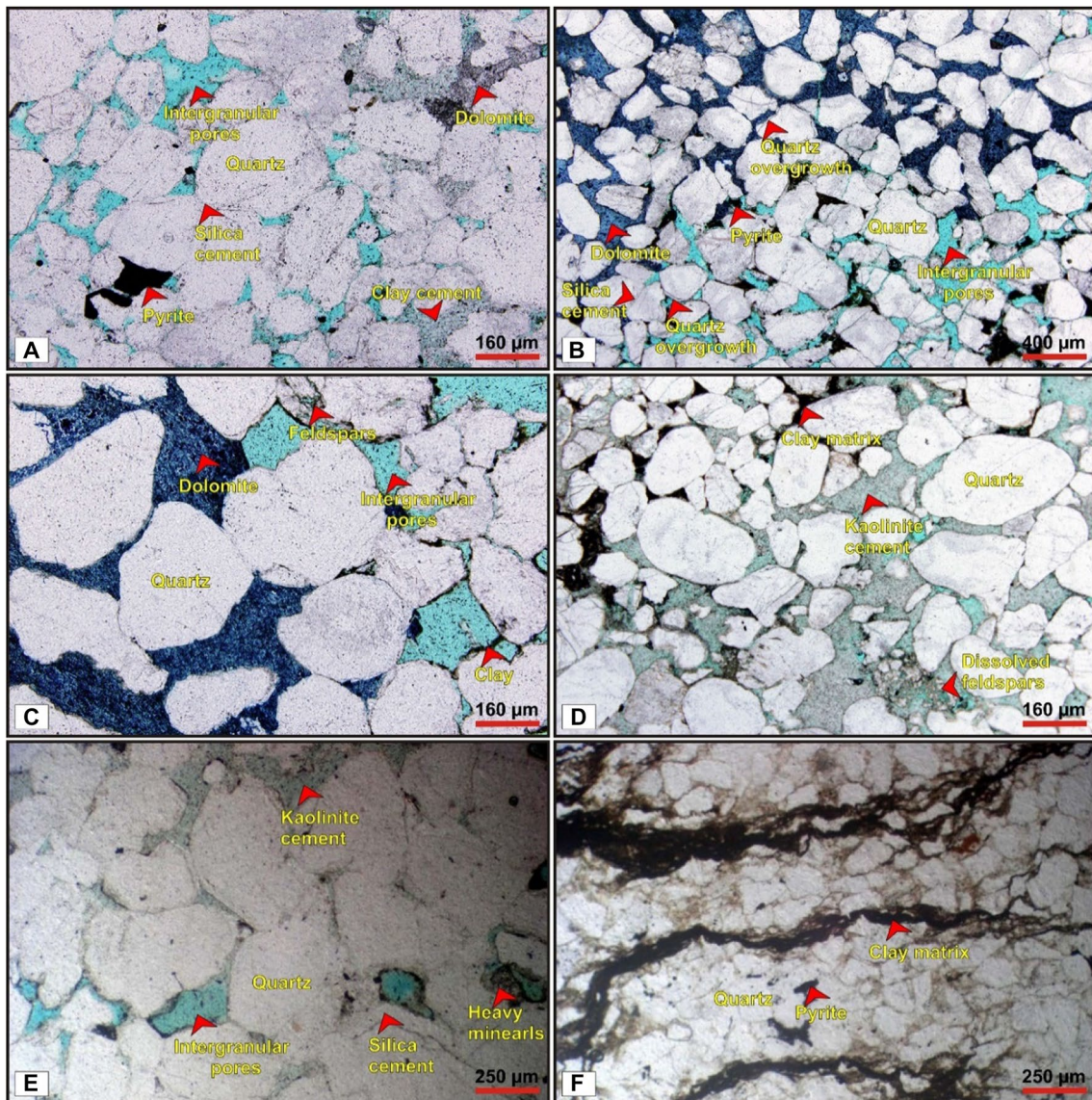


Fig. 10 Thin section microphotographs illustrating the textural and mineralogical composition on the Khatatba sandstone microfacies

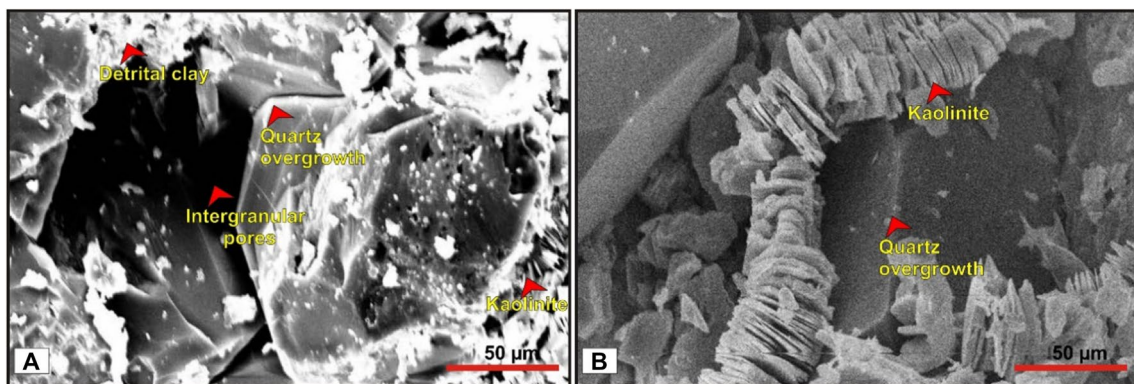


Fig. 11 SEM microphotographs of the Khatatba sandstone microfacies show the pore network structure and pore-occluding mineral phases

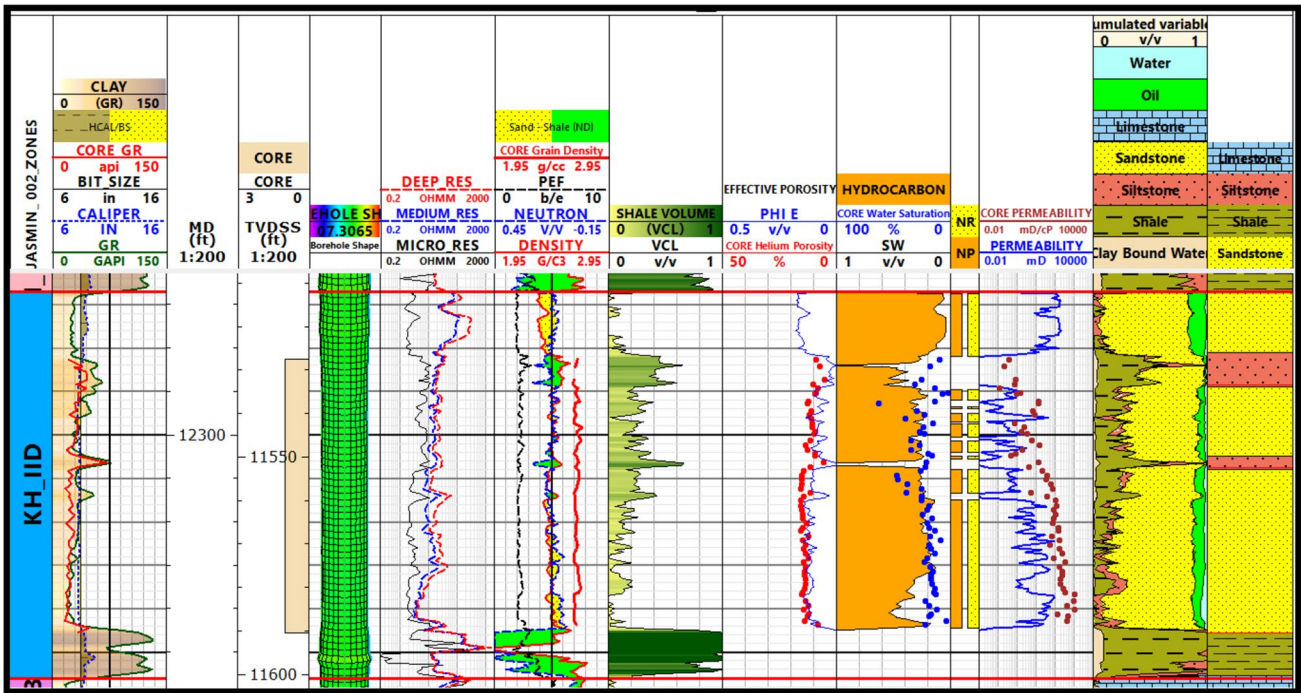


Fig. 12 Lithosaturation cross-plot shows movable hydrocarbons existing in the Khatatba Formation sandstones in Jasmin_002 well

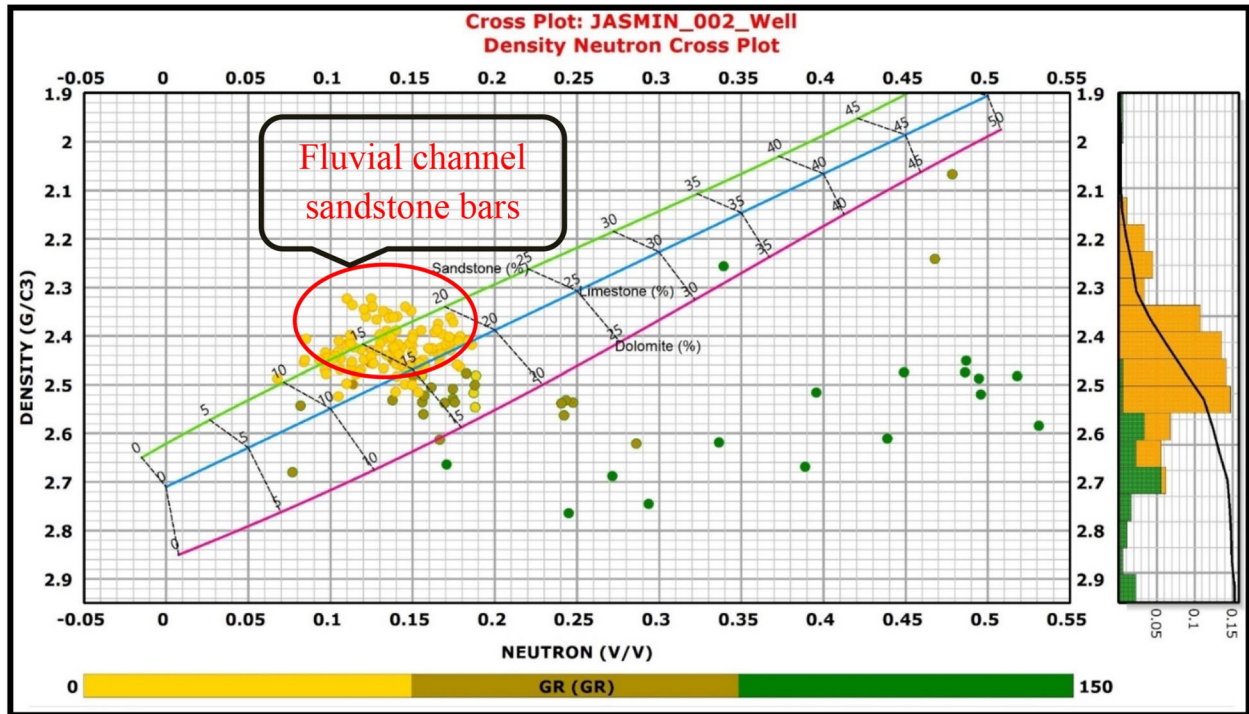


Fig. 13 Neutron-density cross-plot of the cored interval in Jasmin_002 well illustrates the matrix composition of the Khatatba sediments

facies, for example, the abandoned fluvial channel facies, display a flat porosity–permeability curve suggesting the abundance of isolated pores and a tight pore system. The

well-connected pore network of the fluvial channel bars sandstones is also dominated by pore channels with large pore throats (Fig. 14b). Thus, the pore system of the fluvial

Table 2 Petrophysical properties of different sedimentary facies encountered in the cored interval of the Khatatba Formation in Jasmin_002 well

Petrophysical properties	Overbank facies (FA1) (<i>n</i> = 4)			Fluvial channel bars (FA2) (<i>n</i> = 34)			Abandoned channel facies (FA3) (<i>n</i> = 9)			Tidal bars facies (FA4) (<i>n</i> = 9)		
	Minimum	Maximum	Average	Minimum	Maximum	Average	Minimum	Maximum	Average	Minimum	Maximum	Average
H. permeability (mD)	0.49	22.34	10.31	5.30	1112.08	250.20	0.79	15.53	4.48	0.12	13.31	2.79
Porosity (%)	5.63	14.43	10.22	11.50	15.77	14.06	9.33	13.44	10.95	5.18	12.27	9.04
Grain density (g/cm ³)	2.66	2.69	2.68	2.65	2.71	2.67	2.65	2.72	2.67	2.64	2.70	2.66
RQI (μm)	0.07	0.50	0.29	0.21	2.76	1.18	0.09	0.34	0.18	0.04	0.33	0.13
NPI	0.06	0.17	0.12	0.13	0.19	0.16	0.10	0.16	0.12	0.05	0.14	0.10
FZI (μm)	0.69	8.36	3.21	1.64	16.48	7.24	0.74	2.17	1.40	0.43	2.34	1.28
R ₃₅ (μm)	0.56	6.19	3.04	1.92	37.02	14.04	0.68	3.18	1.58	0.27	3.13	1.18

RQI/Reservoir Quality Index, NPI/Normalized Porosity Index, FZI Flow Zone Indicator, R₃₅Pore throat radius

channel bars is characterized by an open, connected pore channel network with wide pore throats. On the other hand, the other sedimentary facies have a tight pore network dominated by isolated probably blocked and/or pore throats.

Reservoir rock typing

The studied Khatatba sedimentary facies have been grouped in three different reservoir rock types (RRTs) with variable petrophysical and sedimentological characteristics (Fig. 15a, b). RRTI consists mainly of fluvial channel bars sandstones having reservoir quality index (RQI) values greater than 1 μm and flow zone indicator (FZI) values above 5 μm (Fig. 15a). RRTI rocks have the best flow properties among all the studied Khatatba facies and are classified as hydraulic flow units HFU5 and HFU6 with FZI values ranging from 5 to 15 μm (Fig. 15a). RRTII sediments include some intervals of the fluvial channel bars facies with fair reservoir characteristics and RQI values in the range of 0.5 μm and 1 μm. RRTII sandstones have also fair hydraulic flow properties with FZI values in the range of 2.5 μm and 5 μm. Therefore, RRTII sediments are classified as HFU4 with fair hydraulic flow characteristics but good storage properties. We hypothesize that the variation in petrophysical properties between RRTI and RRTII sediments is linked to the evolution of their pore structure and network. RRTIII includes all the other sedimentary facies having poor reservoir quality and fluid flow characteristics with average RQI and FZI values of 0.5 μm and 2.5 μm, respectively (Fig. 15a). RRTIII sediments display variable flow capacities and are classified as HFU1, HFU2, and HFU3 (Fig. 15b).

The interpreted RRTs are clustered according to their pore throat radius values (Fig. 16). RRTI sandstones contain large, very well-connected pores with the highest pore throat radius values greater than 10 μm. The large pore throat radii connect the intergranular pores of RRTI, and therefore, no dead ends were observed where the intergranular pore system is dominated by connected, wide pore channel network. The pore throat radius values decrease progressively from RRTI to RRTIII, and the content of dead-end porosity increases in the pore system from RRTI to RRTIII. Notably, RRTII rocks have abundant dead ends; however, some connected pores are still present in the pore system. On the other hand, no connected pores have been observed in RRTIII rocks, and their pore system contains only scattered dead ends. The occurrence of stylolites in RRTII sandstones, which reflect a possible pressure solution, may explain their tighter pore system than that in RRTI rocks. On the other hand, abundance of clay laminae and mud drapes which may act as permeability barriers explains the poor reservoir quality of RRTIII facies (Fig. 16).

The mercury injection capillary pressure (MICP) results reveal a wide variation in the pore system characteristics

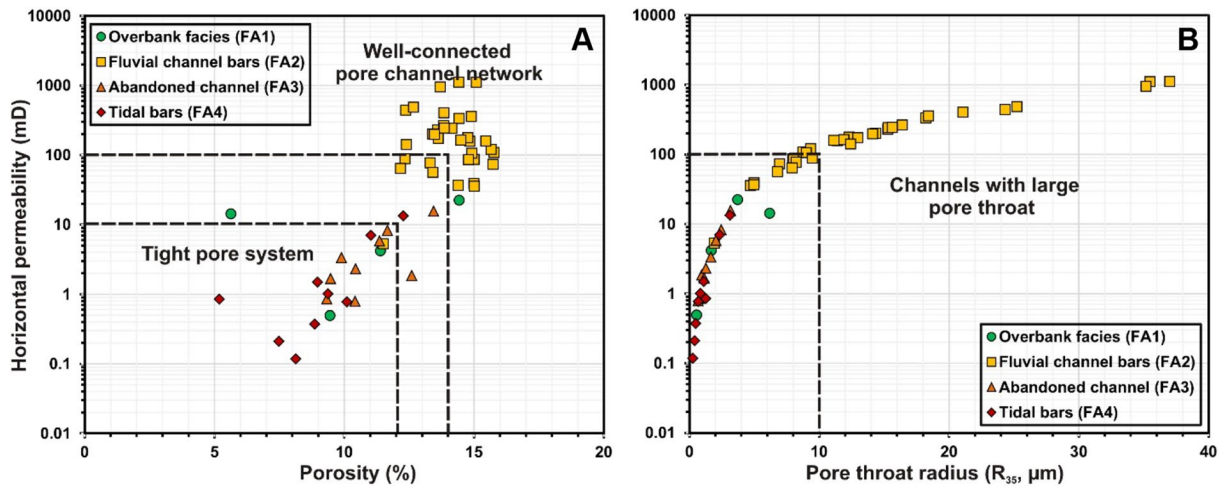


Fig. 14 Horizontal permeability versus helium porosity (A), and pore throat radius (B) cross-plots demonstrate the pore system characteristics in the studied Khatatba sedimentary facies

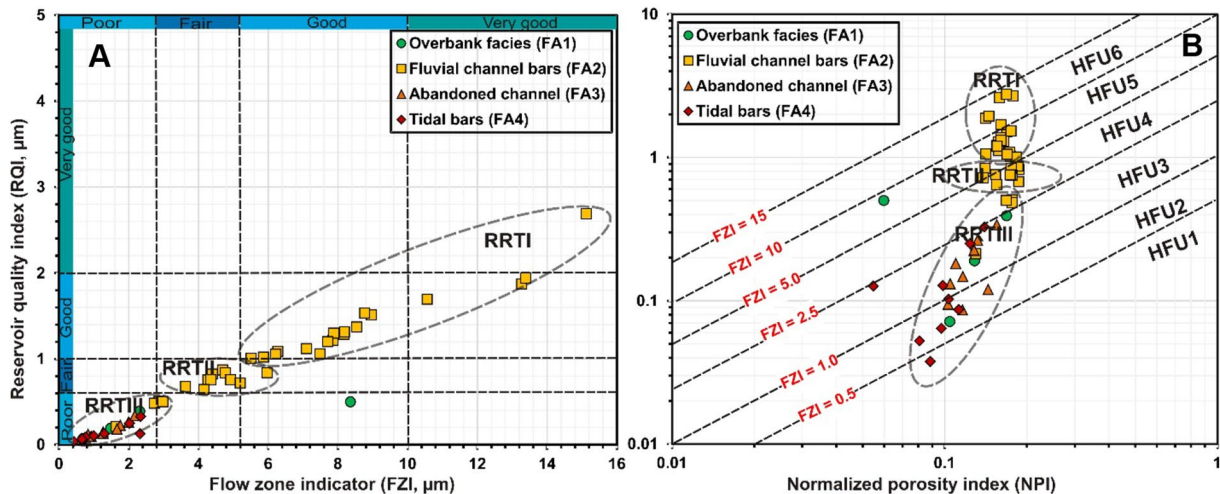


Fig. 15 Reservoir quality index (RQI) versus flow zone indicator (FZI) (A), and normalized porosity index (NPI) (B) cross-plots demonstrating the different rock types encountered in the cored interval of the Khatatba Formation

of the Khatatba RRTs. Capillary pressure versus water saturation cross-plot clearly separates the three interpreted RRTs reflecting the paramount control of their lithological and petrophysical parameters on the entry pressure and hydrocarbon-water displacement. A progressive decrease in water saturation with increasing capillary pressure has been observed in all the Khatatba rock types (Fig. 17a). RRTI sandstones display flat curves parallel to the X-axis from 100% to less than 20% typifying that more than 80% of the pore water can be displaced at low entry pressure levels < 500 psi. On the other hand, RRTII and RRTIII sediments display steeper curves than that in RRTI where in RRTIII less than 50% of the pore water would be displaced at pressure levels < 500 psi. Additionally, the capillary entry

pressure increases progressively from RRTI to RRTIII, and the irreducible water saturation values decrease from RRTIII to RRTI. Notably, irreducible water saturation values of less than 20% are only observed in RRTI rocks.

On the mercury injection capillary pressure “MICP” versus mercury saturation cross-plot (Fig. 17b), greatest volume of mercury up to 80% would intrude the pore system of RRTI rocks at capillary pressure levels less than 100 psi. Furthermore, the capillary entry pressure values in RRTI sandstones are twofold greater than those in RRTII and RRTIII sediments. Such variation in the volume of intruded mercury reflects the abundance of dead ends and irreducible water in RRTII and RRTIII sediments. The MICP curves versus water and mercury saturations demonstrate that the

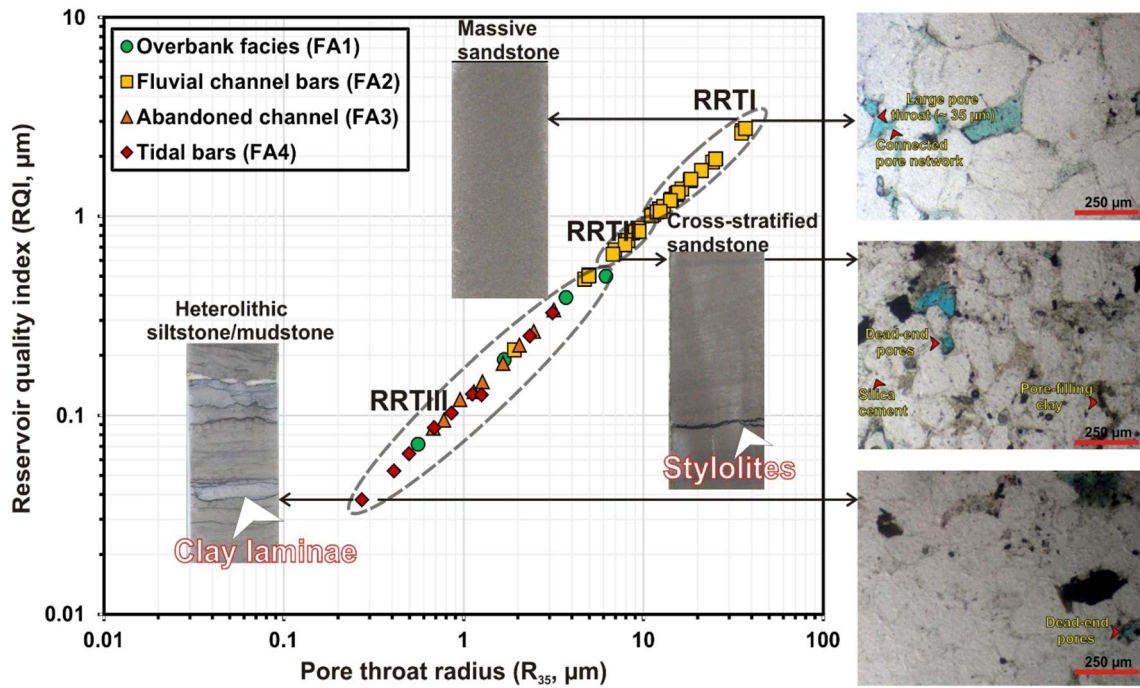


Fig. 16 Pore throat radius (R_{35}) versus reservoir quality index (RQI) cross-plot illustrates the variation in pore system characteristics in the Khatatba reservoir rock types. Core photographs and thin sections

highlight wide variations in sediment composition and microscale pore network among the Khatatba reservoir rock types

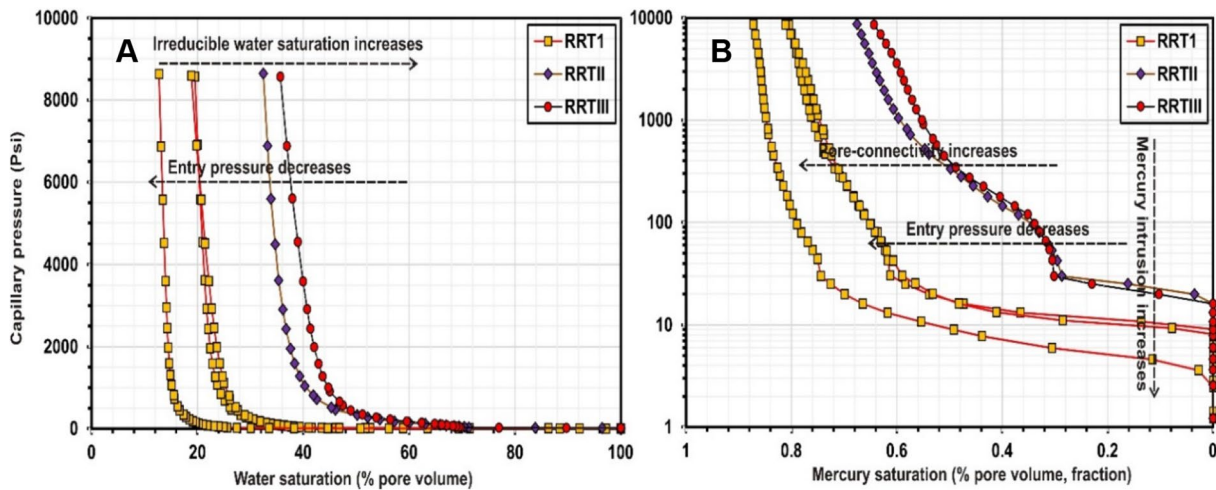


Fig. 17 Mercury injection capillary pressure versus water saturation (A) and mercury saturation (B) demonstrating the variation in pore system properties of the Khatatba reservoir rock types

pore system connectivity and pore geometry, structure, and network differ significantly in the studied RRTs. However, the best pore system properties for optimized reservoir performance are observed in RRTI rocks.

The measured pore throat radius values and their distribution reveal that the RRTI sandstones display a unimodal pore throat size distribution (PTSD) with one maxima observed in the range of 10 μm and 100 μm (Fig. 18a). Such distribution

aligns with the dominance of mega- and super-capillary pores in RRTI sediments, while a bimodal distribution of pore throats has been observed in RRTII and RRTIII rocks with two maxima in the range of macropores and mesopores. Notably, sub-capillary pores/micropores ($<0.1 \mu\text{m}$) are more abundant in the pore system of RRTII and RRTIII than in RRTI where the micropores represent less than 5% of the pore system. The pore throat size distribution versus

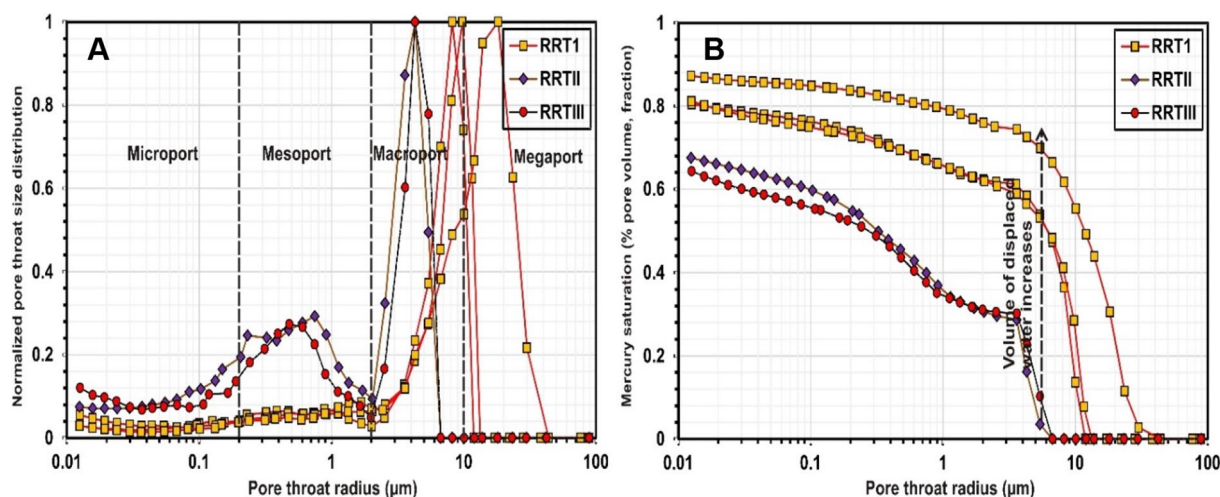


Fig. 18 Pore throat size distribution in the Khatatba reservoir rock types (A), and pore throat radius versus mercury saturation (B) highlighting the dominant pore size in each RRT as well as the impact of pore throat size on mercury intrusion

mercury saturation highlights the prominent variation in the mechanism of mercury intrusion in the Khatatba RRTs (Fig. 18b). The presence of capillary and super-capillary pores ($> 10 \mu\text{m}$) in RRTI facies results in a quick displacement of pore water where more than 80% of the pore water would be displaced by mercury. On the other hand, mercury would only displace 60% of the pore water in RRTII and RRTIII rocks due to the absence of super-capillary pores.

Discussion

Compositional controls on reservoir performance

Primary (rock texture and detrital mineralogy) and secondary (authigenic mineralogy) compositional attributes often induce large-scale heterogeneities on the reservoir quality and pore system characteristics (e.g. Pittman and Larese 1991; Houseknecht and Ross 1992; Pittman 1992; Ehrenberg 1993; Tournier et al. 2010). Several studies have demonstrated that some specific compositional attributes (e.g. clays) can accelerate the pore volume reduction and pore throat blockage during compaction (Houseknecht 1987; Wilson and Stanton 1994), while the dominance of some mineral phases such as quartz and scattered carbonate cement often supports the facies-framework against mechanical compaction and pore network reduction (Leila and Moscariello 2018; Leila and Moscariello 2019; El Adl et al. 2021; Leila and Mohamed 2020).

A wide heterogeneity in the reservoir characteristics has been observed in the studied Khatatba facies. A prominent variation in pore system characteristics is correlated with variation in sedimentary facies (Fig. 19). Some sedimentary facies are enriched in specific mineral phases which

influence their pore system properties. For example, clays are more abundant in the overbank and abandoned channel facies, which are classified as RRTII and RRTIII rocks with tight pore system. Furthermore, quartz content is high in the fluvial channel bars sandstones which are mostly classified as RRTI.

All the reservoir quality parameters (RQI, FZI, and R_{35}) decrease from RRTI to RRTIII. This is consistent with an increase in the clay volume and decrease in quartz content (Fig. 19). RRTI sandstones have the lowest content of silica cement ($< 10\%$), while the content of silica cement increases in the other RRTs (Fig. 20a). Notably, sandstones with silica cement content greater than 10% often exhibit permeability values less than 100 mD. Silica represents the most porosity-destructive cement in siliciclastic reservoirs as it often blocks the entire intergranular volume (Ehrenberg 1993; Leila et al. 2021). Thus, the emergence of silica cement in sandstones is commonly accompanied by a significant decrease in the pore throat size, and hence the pore system connectivity. In RRTI sandstones, the wide range of permeability values (1000–100 mD) is clearly attributed to the relative abundance of silica cement (Fig. 20a). This explains the tight pore system in the stylolite-rich sandstones (Fig. 16).

Analogue to silica cement, a progressive decrease in permeability with increasing carbonate cement content has been observed in all the studied Khatatba RRTs (Fig. 20b). However, the impact of carbonate cement on the fluid flow capacity is more pronounced in RRTIII sandstones. RRTI and RRTII sandstones with carbonate cement contents $< 2\%$ display permeability values greater than 100 mD. Furthermore, the carbonate-rich samples with cement contents $> 5\%$ often have permeability values less than 50 mD.

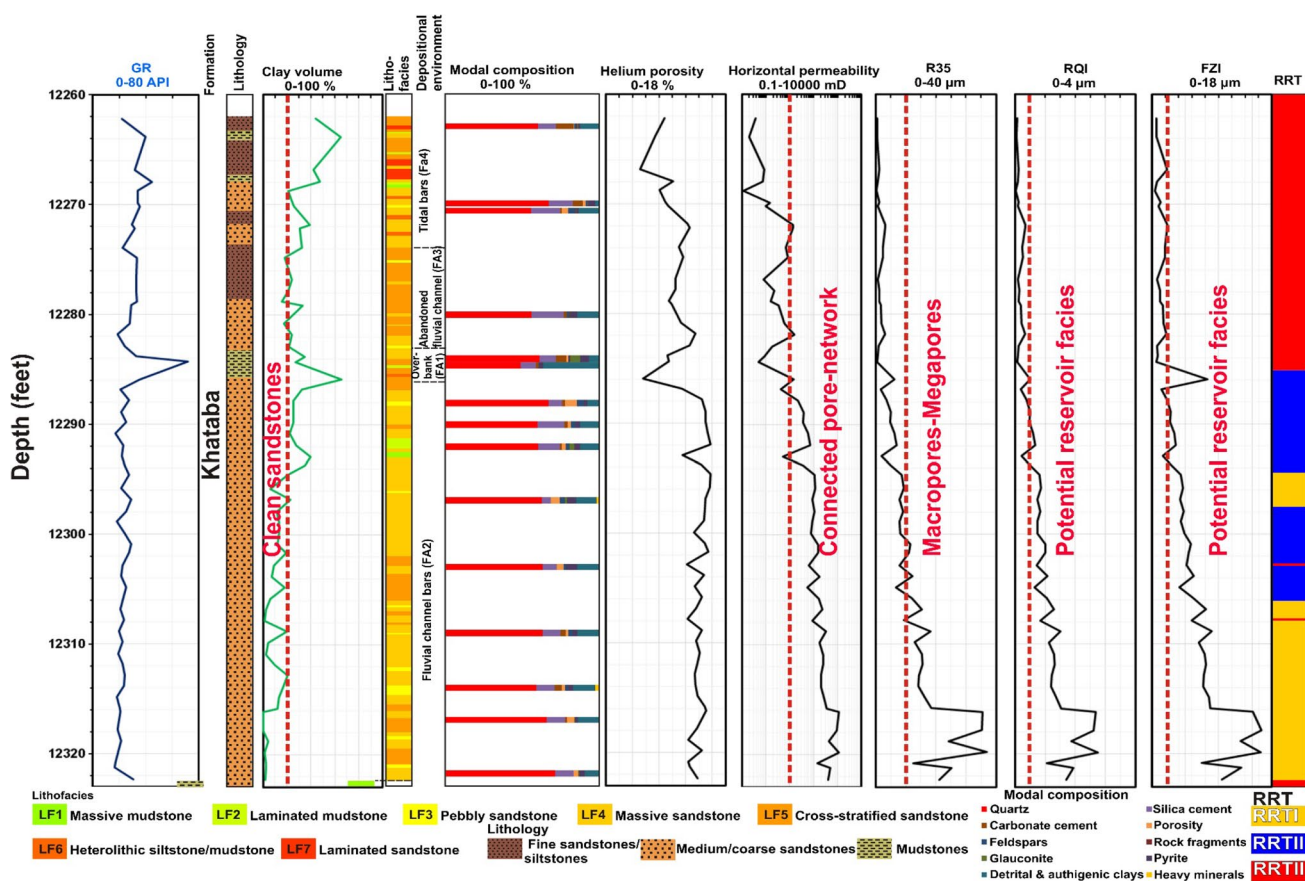


Fig. 19 Distribution of the identified lithofacies and rock types in the studied Khatatba Formation correlated with their mineralogical composition and petrophysical properties

Detrital and authigenic clays display a composite trend with horizontal permeability where the latter initially increases with increasing the clay content before decreasing progressively as clay content increases above a threshold of 10% (Fig. 20c). Similar trends have been described in several publications due to the impact of clay coatings in inhibiting silica cementation, thereby allowing the preservation of the primary intergranular porosity and flow efficiency (e.g. Pittman 1992; Bloch et al. 2002; Tournier et al. 2010; Leila 2019; Leila et al. 2022a, b), while the decreasing trend is most likely attributed to the emergence of thick clay coatings in the intergranular pores, thereby blocking the pore system connectivity, thus creating a pore network dominated by scattered dead ends. Comparing permeability versus silica cement and clay content curves demonstrates the impact of clay coatings on silica cement authigenesis. Additionally, emergence of scattered dead ends in the sandstone samples with abundant clay contents is consistent with the proposed detrimental impact of clays on the sandstone pore system (Figs. 10e, f, 15). This aligns with capillary pressure results, which confirmed the abundance of meso- and micropores in the clay-rich RRTIII facies.

The content of pyrite has a minimal influence on the permeability of the Khatatba RRTs where no distinctive trend is observed in all the studied samples (Fig. 20d). Analogue to the other mineral phases, sandstones with the highest permeability values have the lowest content of pyrite. Therefore, we hypothesize that the sandstones with the highest permeability values display a clean intergranular volume with minimal contents of silica cement, carbonate, clays and pyrite. Clay- and pseudomatrix-rich sandstones are more prone to porosity reduction due to mechanical compaction (Ehrenberg 1990; Midtbø et al. 2000; El Adl et al. 2021; Nabawy et al. 2023). This has been confirmed by the porosity and permeability versus confining pressure curves which demonstrated a significant reduction in the pore volume and pore network connectivity as pressure increases from 400 to 7000 psi (Fig. 21a, b). RRTI rocks display a slightly flat $\varnothing-K$ versus confining pressure curves signifying a mild pore volume reduction and blockage of the pore throat due to compaction. On the other hand, RRTII and RRTIII sandstones display steeper curves relative to RRTI rocks with an approximate 10% reduction in the pore volume as pressure increases from 400 to 7000 psi. The variation in confining

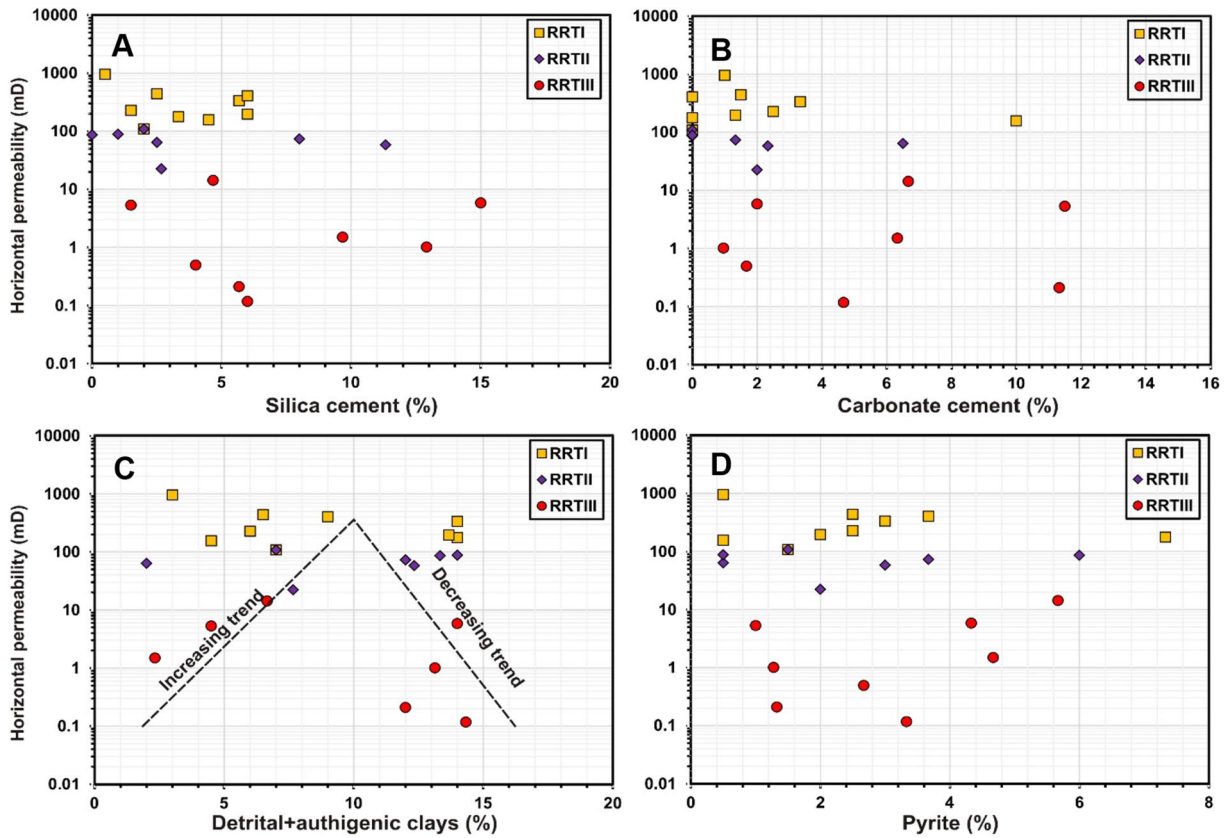


Fig. 20 Cross-plots illustrating the influence of specific compositional attributes on the permeability of the studied Khatatba reservoir rock types

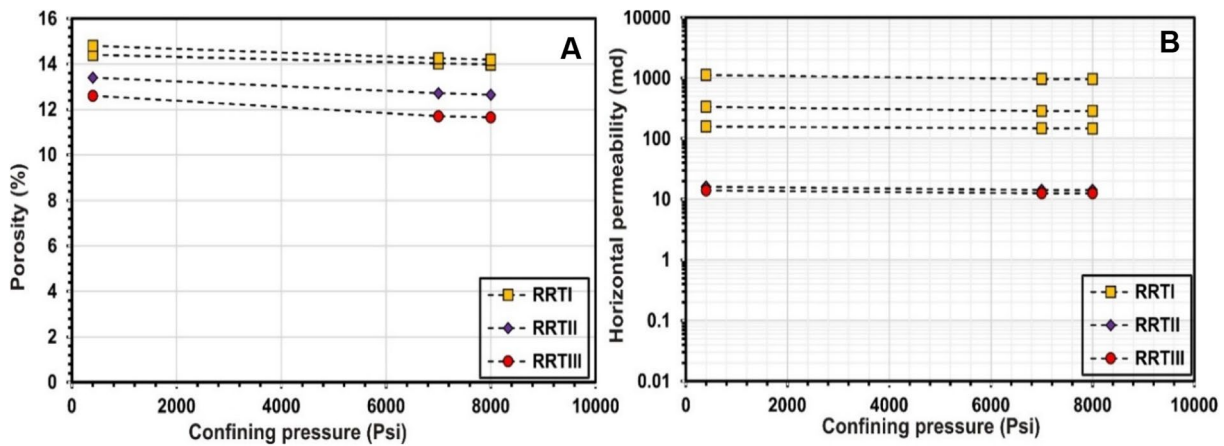


Fig. 21 Confining pressure versus porosity (A), and permeability (B) cross-plots demonstrating the impact of compaction on pore system of the Khatatba reservoir rock types

pressure-porosity and permeability curves among the Khatatba RRTs is attributed to their mineralogical composition where the quartzose framework of the RRTI sandstones would resist compaction, and hence pore volume reduction. On the other hand, ductile materials (e.g. clays, pseudomatrix) abundant in RRTII and RRTIII rocks are often squeezed

between the rigid framework grains, thereby blocking the intergranular volume and pore throats. Thus, the compositional attributes also control the ability of RRTs to preserved their initial pore system connectivity up on compaction, and hence their reservoir potentiality in the deeply buried stratigraphic successions.

Depositional controls: prediction of the best reservoir facies

Initial depositional attributes influencing the eodiagenetic pathways induce paramount controls on the pore system evolution (e.g. De Ros et al. 1994; Kim et al. 2007; Leila and Moscariello 2019; Leila et al. 2023a, b). Early emergence of specific diagenetic phases is restricted to specific depositional environments. For example, the pre-compactional carbonate and glauconite authigenesis was reported in shallow marine sandstones (e.g. Worden and Morad 2003; Kim et al. 2007; Leila and Moscariello 2019). Moreover, some clay mineral phases and pseudomatrix materials tend to concentrate in the low-energy fluvio–deltaic and estuarine facies (De Ros et al. 1994; El Adl et al. 2021; Leila et al. 2021). Petrophysical characteristics and reservoir quality of the Khatatba RRTs show a significant reservoir heterogeneity where the distribution of the RRTs is largely influenced by the depositional facies (Fig. 19). Previous studies reported a wide variation in the Khatatba Formation facies along the major faults where repeated variation in fault offset triggers accumulation of successive progradational and aggradational–retrogradational sedimentary successions (Leila et al. 2022a). Local structural highs and lows are reported in the study region (Fig. 5); however, the Khatatba facies displays a gradual thickening norward without any prominent variation in thickness along the faults (Fig. 6). Thus, a lateral variation in sedimentary facies architecture along the fault patterns is not obvious in the study region. However, interpreted seismic profiles demonstrated a lateral variation in seismic facies where the well-bedded seismic reflections in the study region change into chaotic facies southward (Fig. 3), thereby a southward decrease in the reservoir quality is assumed.

On the stratigraphic modified Lorenz plot (SMLP), RRTIII sediments display a flat curve parallel to the storage capacity axis (Fig. 22a). This behavior is due to abundance of micro-capillary pores in the RRTIII sediments, which are able only to store fluids without obvious contribution to the flow capacity. RRTIII sediments are often restricted to the overbank, tidal bars and abandoned channel facies. RRTII sandstones display a steeper SMLP curve compared with RRTIII sandstones where the former contribute to more than 30% of the Khatatba reservoir storage but accounts only for 15% of the reservoir flow capacity. This is mostly attributed to the occurrence of sub-capillary and capillary pores in RRTII sandstones. Therefore, RRTIII and RRTII sandstones are, respectively, classified as fluid flow barriers and baffle zones. This is consistent with the MICP data, and the classification of RRTII and RRTIII facies as HFU1–HFU4 units.

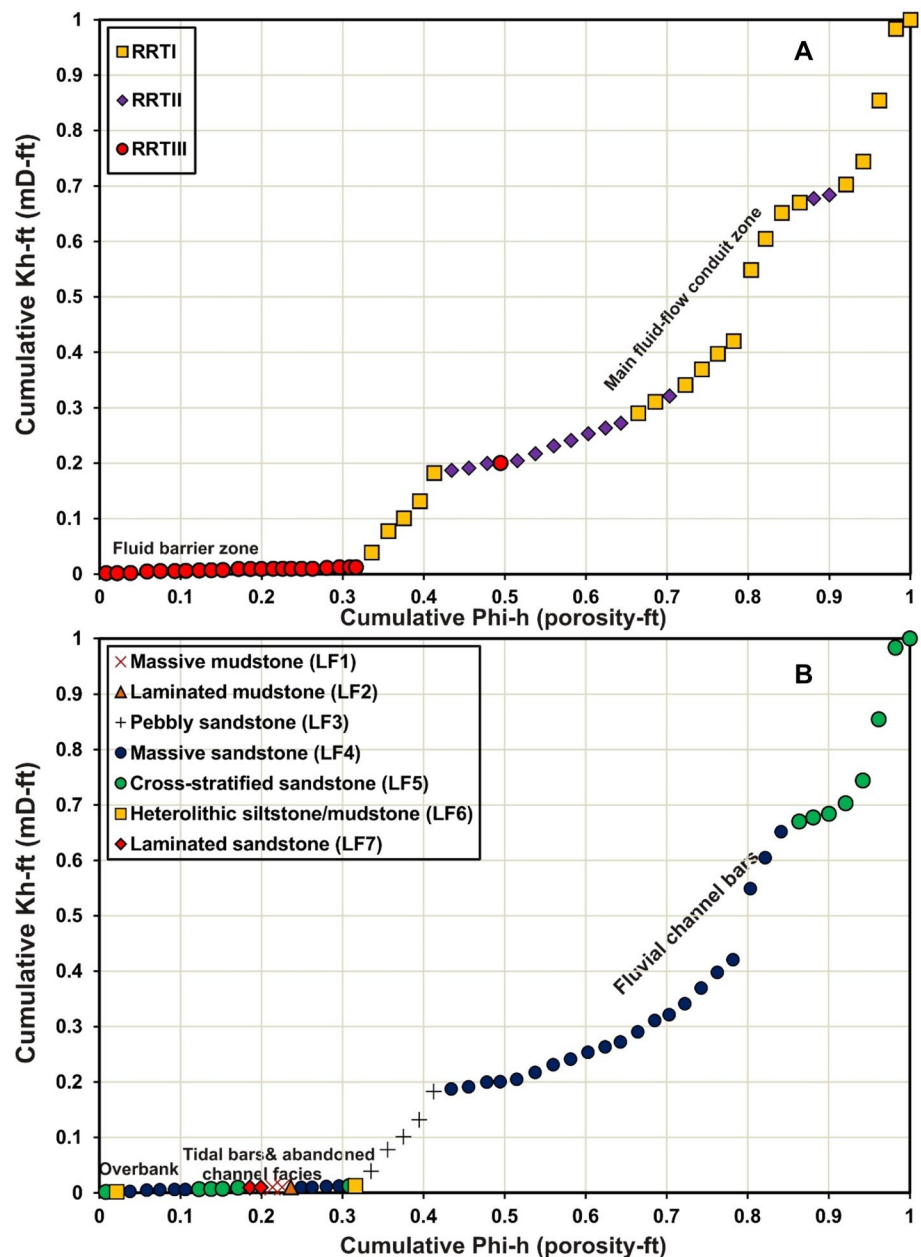
RRTI sandstones display a steep SMLP curve where they contribute to 40% of the Khatatba reservoir storage and more than 80% of its flow capacity (Fig. 22a). Excellent flow capacity of RRTI rocks is largely due to their well-connected

pore system consisting of super-capillary pores. Notably, better reservoir quality sandstones are often associated with pebbly and massive sandstones lithofacies. Additionally, the transition from these lithofacies to the laminated sandstone or heterolithic siltstone/mudstone lithofacies results in a change in the reservoir rock type from RRTI into RRTII or RRTIII (Fig. 22b). Moreover, some lithofacies such as cross-stratified sandstones and laminated sandstones are relatively enriched in clays when associated with a specific sedimentary facies (tidal bars and abandoned channel facies). Therefore, the transition from fluvial channel bars into any other sedimentary facies would result in a shift in the reservoir quality from RRTI to RRTII and RRTIII. Thus, a reduction in the hydrodynamic energy from fluvial channel to overbank or abandoned channel, as well as increasing the marine influence, and transition into tidally influenced environment would result in decreasing the reservoir quality. Hence, any variation in the depositional context and sedimentary facies is usually accompanied by a progressive shift in the reservoir quality and reservoir rock type.

Conclusions

- Seismic-stratigraphic, sedimentological, and petrophysical approaches were integrated to identify the different reservoir rock types (RRTs) encountered in the Middle Jurassic Khatatba Formation and decipher the controls on the evolution of their pore system.
- Khatatba cored interval displays a fining-upward succession where the sedimentary facies changes from fluvial to tidally influenced sediments. The reservoir quality decreases upward where the best reservoir facies coincide with the fluvial channel sand bars.
- Three RRTs were identified in the Khatatba cores. The pore system characteristics of each RRT are largely influenced by both depositional and compositional attributes.
- Fluvial channel bars facies mainly constitute clean quartz arenite sandstones having a well-connected intergranular pore system and contain super-capillary pores ($> 10 \mu\text{m}$). These sandstones have the best flow properties (HFU5 and HFU6) and preliminary classified as RRTI which contributes to more than 95% of the Khatatba reservoir flow capacity.
- RRTII, RRTIII rocks are common in the abandoned channel, overbank, and tidal bars facies. These rock contain abundant pseudomatrix materials, clay, and carbonate cements. RRTII, RRTIII pore system is dominated by sub-capillary pores with high irreducible water saturation content ($\sim 40\%$).
- Mineralogical and lithofacies composition of RRTI rocks characterized by a minimal content of clays and pseu-

Fig. 22 Stratigraphic modified Lorenz plot (SMLP) illustrating the storage and flow capacities of the Khatatba RRT (a), and lithofacies (b) in Jasmin_002 well



domatrix materials prompted the preservation of their initial pore network even at great depths (> 12,000 ft).

- The best reservoir facies within the Khatatba sediments are associated with the high energy fluvial regimes where the RRTs with excellent petrophysical characteristics exist in the fluvial channel bars, which host the main fluid flow conduits.

Acknowledgements The authors are grateful to the Egyptian General Petroleum Corporation (EGPC) and Agiba Petroleum Company for granting the raw data to conduct this research. Thanks to Corex Service Company in Egypt for providing the facilities to carry out this research. The authors are also grateful to Schlumberger for providing access to

the academic license of the Techlog software (TL.2015.3) utilized in this study. The authors are also grateful for the Editor-in-Chief, the associate Editor, and the anonymous reviewers for their valuable and constructive comments that improved the present manuscript in much better version.

Funding Open access funding provided by The Science, Technology & Innovation Funding Authority (STDF) in cooperation with The Egyptian Knowledge Bank (EKB). The authors declare that they did not receive any funding to perform this work.

Declarations

Conflict of interest The authors want to declare that they do not have any conflict of interests to disclose.

Open Access This article is licensed under a Creative Commons Attribution 4.0 International License, which permits use, sharing, adaptation, distribution and reproduction in any medium or format, as long as you give appropriate credit to the original author(s) and the source, provide a link to the Creative Commons licence, and indicate if changes were made. The images or other third party material in this article are included in the article's Creative Commons licence, unless indicated otherwise in a credit line to the material. If material is not included in the article's Creative Commons licence and your intended use is not permitted by statutory regulation or exceeds the permitted use, you will need to obtain permission directly from the copyright holder. To view a copy of this licence, visit <http://creativecommons.org/licenses/by/4.0/>.

References

- Abdelmaksoud A, Radwan AA (2022) Integrating 3D seismic interpretation, well log analysis and static modelling for characterizing the Late Miocene reservoir, Ngatoro area, New Zealand. *Geomech Geophys Geo Energy Geo Resour* 8(2):1–31
- Abdelwahhab MA, Radwan AA, Mahmoud H, Mansour A (2022) Geophysical 3D static reservoir and basin modeling of a Jurassic estuarine system (JG-Oilfield, Abu Gharadig basin, Egypt). *J Asian Earth Sci* 225:105067
- AlSharhan AS, Abd El-Gawad EA (2008) Geochemical characterization of potential Jurassic/cretaceous source rocks in the Shushan Basin, north western Desert Egyptian. *J Pet* 31:191–212
- Amaefule JO, Altunbay M, Tiab D, Kersey DG, Keelan DK (1993) Enhanced reservoir description; using core and log data to identify hydraulic (flow) units and predict permeability in uncured intervals/wells: formation evaluation and reservoir geology. In: *Proceeding Society of Petroleum Engineers Annual Conference*. v. Omega, pp 205–220
- Ayyad MA, Darwish M (1996) Syrian arc structures: a unifying model of inverted basins and hydrocarbon concurrencies in North Egypt. In: *EGPC 13th exploration and production conference vol 1*, pp 40–59
- Baker VR (1987) Paleoflood hydrology and extraordinary flood events. *J Hydrol* 96:79–99
- Bayoumi T (1996) In the influence of interaction of depositional environment and syndepositional tectonics on the development of some Late Cretaceous source rocks, Abu Gharadig basin, Western Desert, Egypt. In: *EGPC 13th exploration and production conference vol 2*, pp 475–496
- Bhattacharya J, Walker RG (1991) Facies and facies successions in river- and wave-dominated depositional systems of the Upper Cretaceous Dunvegan Formation, northwestern Alberta. *Bull Can Pet Geol* 39:165–191
- Blatt H, Tr RJ (1996) *Petrology: igneous, sedimentary, and metamorphic*, 2nd edn. Freeman & Co., New York
- Bloch S, Lander RH, Bonnell L (2002) Anomalously high porosity and permeability in deeply buried sandstone reservoirs: origin and predictability. *AAPG Bull* 86:301–328
- Bosworth W, Tari G (2020) Hydrocarbon accumulation in basins with multiple phases of extension and inversion: examples from the Western Desert (Egypt) and the western Black Sea. *Solid Earth* 12(1):59–77
- Bosworth W, El-Hawat AS, Helgeson DE, Burke K (2008) Cyrenaican “shock absorber” and associated inversion strain shadow in the collision zone of northeast Africa. *Geology* 36(9):695–698
- Bridge JS (2006) Fluvial facies models: recent developments. In: Walker RG (ed) *Facies models revisited*. IAS Special Publication, vol 84, pp 85–170
- Coskun SB, Wardlaw NC, Haverslew B (1993) Effects of composition, texture and diagenesis on porosity, permeability and oil recovery in a sandstone reservoir. *J Petrol Sci Eng* 8:219–292
- De Ros L, Morad S, Paim P (1994) The role of detrital composition and climate on the diagenetic evolution of continental molasses: evidence from the Cambro-Ordovician Guaritas Sequence, Southern Brazil. *Sed Geol* 92:197–228
- Dickinson WR (1970) Interpreting detrital modes of graywacke and arkose. *J Sediment Petrol* 40:695–707
- Dolson C, Shaan V, Matbouly S, Harwood C, Rashed R, Hammouda H (2001) The petroleum potential of Egypt. In: Downey W, Threet C, Morgan A (eds) *Petroleum provinces of the twenty-first century*. AAPG Memoir, vol 74, pp 453–482
- EGPC (1994) Nile Delta and North Sinai: field discoveries and hydrocarbon potentials (a comprehensive overview). Egyptian General Petroleum Corporation, Cairo, p 387
- Ehrenberg S (1990) Relationship between diagenesis and reservoir quality in sandstones of the Garn Formation, Haltenbanken, mid-Norwegian continental shelf. *AAPG Bull* 74:1538–1558
- Ehrenberg S (1993) Preservation of anomalously high porosity in deeply buried sandstones by grain coating chlorite: examples from the Norwegian continental shelf. *AAPG Bull* 77:1260–1286
- El Diasty W (2015) Khatatba Formation as an active source rock for hydrocarbons in the northeast Abu Gharadig Basin, north Western Desert, Egypt. *Arab J Geosci* 8(4):1903–1920
- El Adl H, Leila M, Ahmed MA, Anan T, El-Shahat A (2021) Integrated sedimentological and petrophysical rock-typing of the Messinian Abu Madi formation in South Batra gas field, onshore Nile Delta, Egypt. *Mar Petrol Geol* 124:1–28
- El Matboly EA, Leila M, Peters KE, El Diasty WS (2022) Oil biomarker signature and hydrocarbon prospectivity of Paleozoic versus Mesozoic source rocks in the Faghur–Sallum basins, Egypt's Western Desert. *J Petrol Sci Eng* 217:110872
- Elmahdy M, Radwan AA, Nabawy B, Abdelmaksoud A, Nastavkin AV (2023) Integrated geophysical, petrophysical and petrographical characterization of the carbonate and clastic reservoirs of the Waihapa Field, Taranaki Basin, New Zealand. *Mar Pet Geol* 151:106173
- Garfunkel Z (2004) Origin of the Eastern Mediterranean Basin: a re-evaluation. *Tectonophysics* 391:11–34
- Guiraud R, Bosworth W (1997) Senonian basin inversion and rejuvenation of rifting in Africa and Arabia: synthesis and implications to plate-scale tectonics. *Tectonophysics* 282:39–82
- Guiraud R, Bosworth W, Thierry J, Delplanque A (2005) Phanerozoic geological evolution of Northern and Central Africa: an overview. *J Earth Sci* 43:83–143
- Gunter GW, Finneran JM, Hartmann DJ, Miller JD (1997) Early determination of reservoir flow units using an integrated petrophysical method. In: Paper SPE 38679 prepared for presentation at the 1997 SPE annual technical conference and exhibition held in San Antonio, Texas, 5–8 October, pp 1–8
- Guo G, Diaz MA, Paz F, Smalley J, Waninger A (2007) Rock typing as an effective tool for permeability and water-saturation modelling: a case study in a clastic reservoir in the Oriente Basin. *SPE Reserv Eval Eng* 10(6):730–739
- Hassan M, Leila M, Ahmed MA, Issa G, Hegab O (2022) Geochemical characteristics of natural gases and source rocks in Obayed sub-basin, north Western Desert, Egypt: implications for gas-source correlation. *Acta Geochim* 42:241–255
- Houghton H (1980) Refined techniques for staining plagioclase and alkali feldspar in thin section. *J Sediment Petrol* 50:629–631
- Houseknecht DW (1987) Assessing the relative importance of compaction processes and cementation to reduction of porosity in sandstones. *AAPG Bull* 71:633–642
- Houseknecht DW, Ross LM (1992) Clay minerals in Atokan deep-water sandstone facies, Arkoma Basin: origins and influence on

- diagenesis and reservoir quality. In: Houseknecht DW, Pittman ED (eds) Origin, diagenesis, and petrophysics of clay minerals in sandstones. SEPM Special Publication, vol 47, pp 227–240
- Jooybari HS, Mowazi GH, Jaber SR (2010) A new approach for rock typing used in one of the Iranian carbonate reservoir (a case study). In: Paper SPE 131915, international oil & gas conference exhibition, 8–10 June 2010 (Beijing, China)
- Kassab MA, Abbas AE, Attiya AS (2019) Hydrocarbon potential of Upper Bahariya member in Um Baraka oil field, North Western Desert, Egypt. *NRIAG J Astron Geophys* 8(1):204–219
- Keeley ML, Wallis RJ (1991) The Jurassic system in northern Egypt: II. Depositional and tectonic regimes. *J Pet Geol* 14:49–64
- Keeley M, Dungworth G, Floyd C, Forbes G, King C, McGarva R, Shaw D (1990) The Jurassic system in the northern Egypt: I. Regional stratigraphy and implications for hydrocarbon prospectivity. *J Pet Geol* 13:397–420
- Kim J, Yong L, Hisada K (2007) Depositional and compositional controls on sandstone diagenesis, the Tetori Group (Middle Jurassic-Early Cretaceous), central Japan. *Sed Geol* 195:183–202
- Leila M (2019) Clay minerals distribution in the pre-, syn-Messinian salinity crisis sediments of the onshore Nile Delta, Egypt: Mineral origin and implications on the reservoir quality. *J Afr Earth Sci* 154:35–48
- Leila M, Mohamed A (2020) Diagenesis and petrophysical characteristics of the shallow Pliocene sandstone reservoirs in the Shinfas Gas Field, onshore Nile Delta, Egypt. *J Pet Explor Prod Technol* 10:1743–1761
- Leila M, Moscariello A (2018) Depositional and petrophysical controls on the volumes of hydrocarbons trapped in the Messinian reservoirs, onshore Nile Delta, Egypt. *Petroleum* 4:250–267
- Leila M, Moscariello A (2019) Seismic stratigraphy and sedimentary facies analysis of the pre- and syn-Messinian salinity crisis sequences, onshore Nile Delta, Egypt: implications for reservoir quality prediction. *Mar Pet Geol* 101:303–321
- Leila M, Ali E, Abu El-Magd A, AlWaan L, Elgendy A (2021) Formation evaluation and reservoir characteristics of the Messinian Abu Madi sandstones in Farassour gas field, onshore Nile delta, Egypt. *J Pet Explor Prod Technol* 11:133–155
- Leila M, Yasser A, El Bastawesy M, El Mahmoudi A (2022a) Seismic stratigraphy, sedimentary facies analysis and reservoir characteristics of the Middle Jurassic syn-rift sediments in Salam Oil Field, north Western Desert, Egypt. *Mar Pet Geol* 136:105466
- Leila M, El Sharawy M, Bakr A, Mohamed A (2022b) Controls of facies distribution on reservoir quality in the Messinian incised-valley fill Abu Madi Formation in Salma delta gas field, north-eastern onshore Nile Delta, Egypt. *J Nat Gas Sci Eng* 97:104360
- Leila M, Awadalla A, Farag A, Moscariello A (2022c) Organic geochemistry and oil-source rock correlation of the Cretaceous succession in West Wadi El-Rayan (WWER) concession: implications for a new Cretaceous petroleum system in the north Western Desert, Egypt. *J Pet Sci Eng* 219:111071
- Leila M, Moscariello A, Sweet DE, Šegvić B (2023a) Diagenetic signatures in the deltaic and fluvial-estuarine Messinian sandstone reservoirs in the Nile Delta as a tool for high-resolution stratigraphic correlations. *Int J Sedim Res*. <https://doi.org/10.1016/j.ijsrc.2023.05.002>
- Leila M, Sen S, Ganguli SS, Moscariello A, Abioui M (2023b) Integrated petrographical and petrophysical evaluation for reservoir management of the Upper Miocene Qawasim sandstones in West Dikirmis, onshore Nile Delta, Egypt. *Geoenergy Sci Eng* 226:211789
- Leverett MC (1941) Capillary behavior in porous solids. American Institute of Mining and Metallurgical Engineers, Transactions, vol 142, pp 152–169
- Masalmeh SK, Wei L, Hillgartner H, Al-Mjeni R, Blom CR (2012) Developing high resolution static and dynamic models for water-flood history matching and EOR evaluation of a Middle Eastern carbonate reservoir. In: Paper SPE 161485, Abu Dhabi international petroleum conference & exhibition, 11–14 November 2012 (Abu Dhabi, UAE)
- Miall A (1977) A review of the braided river depositional environment. *Earth Sci Rev* 13:1–62
- Miall AD (1996) The geology of fluvial deposits. Springer, Berlin
- Midtbø REA, Rykkje JM, Ramm M (2000) Deep burial diagenesis and reservoir quality along the eastern flank of the Viking Graben. Evidence for illitization and quartz cementation after hydrocarbon emplacement. *Clay Miner* 35:227–237
- Nabawy B, Moustafa A, Radwan AA, Kotb A, Leila M (2023) Seismic reservoir characterization of the syn-rift lower Miocene Rudeis Formation in the July oilfield, Gulf of Suez basin, Egypt: implication for reservoir quality assessment. *Geoenergy Sci Eng* 226:211797
- Nio SD, Yang CS (1991) Sea-level fluctuations and the geometric variability of tide-dominated sandbodies. *Sed Geol* 70(2):161–193
- Pickett GR (1972) Practical formation evaluation. GR Pickett Inc, Golden
- Pittman ED (1992) Relationship of porosity and permeability to various parameters derived from mercury injection-capillary pressure curves for sandstone. *AAPG Bull* 76:191–198
- Pittman ED, Larese RE (1991) Compaction of lithic sands: experimental results and applications. *AAPG Bull* 75:1279–1299
- Poupon A, Leveaux J (1971) Evaluation of Water Saturation in Shaly Formations. *Log Anal* 12:1–2
- Radwan AA, Nabawy B (2022) Hydrocarbon prospectivity of the Miocene-Pliocene clastic reservoirs, Northern Taranaki basin, New Zealand: integration of petrographic and geophysical studies. *J Pet Explor Prod Technol* 12(7):1945–1962
- Radwan AA, Nabawy B, Abdelmaksoud A, Lashin A (2021) Integrated sedimentological and petrophysical characterization for clastic reservoirs: a case study from New Zealand. *J Nat Gas Sci Eng* 88:103797
- Radwan AA, Abdelwahhab MA, Nabawy B, Mahfouz KH, Ahmed MS (2022a) Facies analysis-constrained geophysical 3D-static reservoir modeling of Cenomanian units in the Aghar Oilfield (Western Desert, Egypt): Insights into paleoenvironment and petroleum geology of fluviomarine systems. *Mar Pet Geol* 136:105436
- Radwan AA, Nabawy B, Shihata M, Leila M (2022b) Seismic interpretation, reservoir characterization, gas origin and entrapment of the Miocene-Pliocene Mangaa C sandstone, Karewa Gas Field, North Taranaki Basin. *N Z Mar Pet Geol* 135:105420
- Rose W, Bruce WA (1949) Evaluation of capillary character in petroleum reservoir rock. *Trans AIME* 186:127–142
- Saleh AH, Henaish A, Ramadan F, Abd El Fatah M, Leila M (2023) Petrophysical characterization of the heterogeneous shale-rich oil reservoirs: a case study of the Cenomanian Clastics, Abu Senan Concession, North Western Desert of Egypt. *Arab J Geosci* 16:351
- Schlumberger (1995) Well evaluation conference, Egypt. Schlumberger technical editing services, Chester, pp 58–66
- Shalaby MR, Hakimi MH, Abdullah WH (2011) Geochemical characteristics and hydrocarbon generation modeling of the Jurassic source rocks in the Shushan Basin, north Western Desert, Egypt. *Mar Pet Geol* 28:1611–1624
- Skalinski M, Kenter JAM (2014) Carbonate petrophysical rock typing: integrating geological attributes and petrophysical properties while linking with dynamic behaviour. In: Agar SM, Geiger S (eds) Fundamental controls on fluid flow in carbonates. Geological Society of London, Special Publications, pp 406229–406259
- Swanson BF (1981) A simple correlation between permeabilities and mercury capillary pressures. *J Petrol Technol* 33:2488–2504

- Torfstein A, Steinberg J (2020) The Oligo-Miocene closure of the Tethys Ocean and evolution of the proto-Mediterranean Sea. *Sci Rep* 10(1):13817
- Tournier F, Pagel M, Portier E, Wazir E, Fiet N (2010) Relationship between deep diagenetic quartz cementation and sedimentary facies in a Late Ordovician glacial environment (Sbaa basin, Algeria). *J Sediment Res* 80:1068–1084
- Tucker ME (2001) *Sedimentary petrology*, 3rd edn. Wiley, Oxford
- Varejão FG, Warren LV, Simões MG, Buatois LA, M'angano MG, Bahniuk AM, Assine ML, (2021) Mixed siliciclastic–carbonate sedimentation in an evolving epicontinental sea: Aptian record of marginal marine settings in the interior basins of north-eastern Brazil. *Sedimentology* 68:2125–2164
- Vavra CL, Kaldi JG, Sneider RM (1992) Geological applications of capillary pressure: a review. *AAPG Bull* 76:840–850
- Walling DE, Hu Q (1998) The spatial variability of overbank sedimentation on river floodplains. *Geomorphology* 24:209–223
- Wells JD, Amaefule JO (1985) Capillary pressure and permeability relationships in tight gas sands. In: *SPE 60th Annual Technical Conference* (19–22 May). SPE 13879
- Wescott WA, Atta M, Blanchard DC, Cole RM, Georgeson S, Miller DA, Walter, O'Hayer W, Wilson A, Dolson J, Sehim A (2011) Jurassic rift architecture in the Northeastern Western Desert, Egypt. In: *AAPG international conference and exhibition, Milan, Italy, October 23–26*, pp 1–5
- Wilson MD, Stanton PT (1994) Diagenetic mechanisms of porosity and permeability reduction and enhancement. In: Wilson MD (ed) *Reservoir quality assessment and prediction in clastic rocks*, SEPM, short course, vol 30, pp 59–118
- Winland HD (1972) Oil accumulation in response to pore size changes, Weyburn field, Saskatchewan. Amoco Production Company report F72-G-25 (unpublished), Tulsa, OK, p 20
- Worden R, Morad S (2003) Clay minerals in sandstones: controls on formation, distribution and evaluation. *IAS Spec Publ* 34:3–41
- Yasser A, Leila M, El Bastawesy M, El Mahmoudi A (2021) Reservoir heterogeneity analysis and flow unit characteristics of the Upper Cretaceous Bahariya Formation in Salam Field, north Western Desert, Egypt. *Arab J Geosci* 14(16):1635
- Zein El-Din MY, El-Gawad AA, El-Shayb HM, Haddad IA (2001) Geological studies and hydrocarbon potentialities of the Mesozoic rocks in Ras Kanayis onshore area, northwestern Desert, Egypt. *Ann Geol Surv Egypt* 24:115–134

Publisher's Note Springer Nature remains neutral with regard to jurisdictional claims in published maps and institutional affiliations.